ROYAL SOCIETY OF CHEMISTRY

REVIEW

Check for updates

Copper-based single-atom nanozymes: from fundamental insights to biomedical applications

Dong Peng, [ID] [a] Shanshan Huang, [ID] [a] Mingming Que, [ID] [a] Xiulong Deng, [ID] [a] Zhonggao Zhou [ID] *[a] and Hongdeng Qiu [ID] *[b]

Copper-based single-atom nanozymes (Cu SAzymes) have emerged as a revolutionary class of enzyme mimics, distinguished by their maximized atom utilization efficiency, well-defined active sites, and superior catalytic performance. This review provides a comprehensive overview of the latest advances in Cu SAzymes, systematically outlining their diverse enzyme-like activities, the atomic-level strategies for modulating their catalytic behavior, and their burgeoning applications in biosensing, antibacterial and anticancer therapy, and anti-inflammatory treatment. We emphasize the critical structure-activity relationships that govern their multi-enzyme capabilities and highlight innovative designs that enable synergistic and stimulus-responsive therapies. By establishing a framework that links atomic structure to enzyme-mimicking function and, ultimately, to advanced therapeutic utility, this review not only summarizes the current state of the art but also outlines prevailing challenges and future directions, underscoring the significant potential of Cu SAzymes to drive interdisciplinary innovations in nanobiotechnology and precision medicine.

1. Introduction

Nanozymes, as a class of enzyme-mimicking nanomaterials, have emerged as compelling alternatives to natural enzymes, overcoming inherent limitations such as low stability, high cost, and difficulty in recycling.[1–3] Since the seminal discovery of the intrinsic peroxidase (POD)-like activity of Fe_3O_4 nanoparticles, the field has witnessed an explosive growth, evolving from simple nanoparticle-based mimics to sophisticated nanostructures with tailored functionalities.[4] Among these advancements, single-atom nanozymes (SAzymes), which feature atomically dispersed metal active sites anchored on solid supports, have emerged as a new generation of artificial enzymes that combine high catalytic efficiency with exceptional structural stability.[5,6] By maximizing atom utilization efficiency and offering well-defined coordination environments, SAzymes bridge the gap between natural enzymes and conventional nanozymes, demonstrating superior activity and selectivity in diverse catalytic reactions.[7–9] Since the concept was introduced in 2019, SAzymes have rapidly evolved into a vibrant research frontier, with applications spanning biomedical therapy, biosensing, and environmental catalysis.[10]

Among various metal-based SAzymes, copper-based single-atom nanozymes (Cu SAzymes) exhibit distinctive advantages owing to their versatile enzyme-mimicking capabilities and unique physicochemical properties.[11–15] Cu SAzymes can mimic a broad spectrum of natural enzymes, including POD, oxidase (OXD), superoxide dismutase (SOD), and catalase (CAT), often within a single material system.[16–19] Their catalytic behavior is highly tunable through coordination engineering, enabling precise control over substrate specificity and reaction kinetics. Beyond single-atom systems, copper-based molecular catalysts and nanocomposites represent complementary approaches to enzyme mimicry.[20–22] The molecular catalysts typically offer a clearer definition of the active site and mechanism, but may face challenges in terms of physiological stability; while Cu SAzymes utilize a robust metal-support coordination to exhibit good durability in biological environments, their active site accessibility and catalytic turnover rate can be affected by the solid support. Additionally, their size determines different application modes; small molecules facilitate diffusion and penetration, while nanozymes can achieve targeting and multifunctional integration. The essential biological role of copper in redox homeostasis and metalloenzyme function makes Cu SAzymes particularly suitable for biomedical applications, such as antibacterial activity, anticancer therapy, and inflammatory regulation.

Despite rapid progress, current research on Cu SAzymes remains largely fragmented, often concentrating on isolated enzyme activities or particular applications, which has left significant knowledge gaps. Broad nanozyme reviews have extensively summarized the catalytic mechanisms, classification, and biomedical applications of diverse nanozymes across

[a] College of Chemistry and Materials Science, Gannan Normal University, Ganzhou 341000, China

[b] Key Laboratory of Rare Earths, Ganjiang Innovation Academy, Chinese Academy of Sciences, Ganzhou 341119, China

metal oxides, metal nanoparticles, carbon-based nanostructures, and MOFs, but they typically discuss copper systems only briefly as part of larger material categories.[14,23–27] Similarly, recent general SAzyme reviews emphasize the conceptual evolution, synthesis strategies, and universal coordination-activity relationships of single-atom catalysts, yet they seldom provide an in-depth analysis of copper-based SAzymes as an independent subclass.[28–33] A few copper-focused nanozyme reviews have emerged, but they mainly describe Cu-based nanoparticle or cluster systems, lacking an atomically resolved discussion of single-atom Cu coordination environments and their multi-enzyme behaviors.[34,35] A comprehensive review that classifies their multi-enzyme activities, elucidates the structure-function relationships at the atomic level, and explores their potential in combined therapeutic strategies is therefore urgently needed.

This review aims to provide a comprehensive and up-to-date overview of the rational design, catalytic mechanisms, and emerging applications of Cu SAzymes, which is structured around a unifying framework that connects atomic-level engineering to macro-level biomedical efficacy (Fig. 1). Firstly, we systematically classified and rationalized the multi-enzyme activities of Cu SAzymes under a coherent mechanistic umbrella, linking specific coordination environments to their catalytic performance. Then, we elucidated the structure–activity relationships at the atomic scale, demonstrating how deliberate engineering of the copper center's coordination sphere and the supporting matrix dictates selectivity, activity, and stimulus-responsiveness. Furthermore, we integrated these fundamental insights into innovative therapeutic applications (including antibacterial therapy, anticancer treatment, biosensing, and anti-inflammatory interventions), showcasing how the tunable multi-enzyme properties of Cu SAzymes enable synergistic and smart therapeutic strategies. Finally, we outline current challenges and prospects, including clinical translation, biocompatibility optimization, and intelligent therapeutic systems. Together, this review provides an integrative and design-oriented roadmap that advances the understanding and engineering of Cu SAzymes beyond what has been presented in existing reviews, providing a roadmap for the rational design of next-generation-specific SAzymes.

2. Diverse enzyme-like activities of Cu SAzymes

Cu SAzymes have distinguished themselves in the nanozyme landscape not merely by replicating individual enzyme functions, but by exhibiting a broad and tunable catalytic repertoire. This versatility stems from their atomically dispersed copper centers, whose coordination environment can be precisely engineered to mimic a spectrum of natural enzymes, including POD, CAT, OXD, and SOD, and even more specialized oxidoreductases like laccase, galactose oxidase (GAO), glutathione oxidase (GSHOx), L-cysteine oxidase (LCO), and NADH oxidase (NOx). This chapter systematically illustrates the catalytic processes and mechanisms for different enzyme-like activities.

2.1 POD-like activity

Cu SAzymes have emerged as highly efficient POD mimics owing to their atomically dispersed active centers. Compared with natural horseradish peroxidase (HRP), Cu SAzymes not only maximize metal utilization but also provide flexible regulation over hydrogen peroxide (H_2O_2) activation, enabling the controlled generation of reactive oxygen species (ROS).

The POD-like catalysis of Cu SAzymes generally follows a Fenton-like process. H_2O_2 molecules adsorb onto the Cu active site, where electron transfer between the Cu center and its coordination ligands weakens the O–O bond. Cleavage of this bond yields hydroxyl radicals ($^{\bullet}$OH) or surface-bound *OH intermediates that oxidize chromogenic substrates such as 3,3′,5,5′-tetramethylbenzidine (TMB), o-phenylenediamine (OPD), or 2,2′-azino-bis(3-ethylbenzothiazoline-6-sulfonic acid) (ABTS). Evidence for this pathway has been confirmed through ESR spectroscopy, fluorescence probes, and density functional theory (DFT) studies, which consistently show that unsaturated Cu sites lower the energy barrier for O–O bond dissociation (Fig. 2A and B).[36–38] Kinetic analyses highlight the superior performance of Cu SAzymes compared with nanoparticle-based catalysts. For example, Cu-N$_4$/S-rGO exhibits k_{cat}/K_m values nearly 2500 times greater than pristine rGO (Fig. 2C),[39] while Cu-SAZs encapsulated in platelet membranes achieve Michaelis constant (K_m) and maximum reaction rate (V_{max}) values comparable to natural PODs.[40]

2.2 OXD-like activities

Cu SAzymes exhibit remarkable OXD-like activity, enabling the catalytic oxidation of various substrates without the need for H_2O_2. This section delves into the general OXD-like activity of Cu SAzymes and their specific activities toward distinct target substrates.
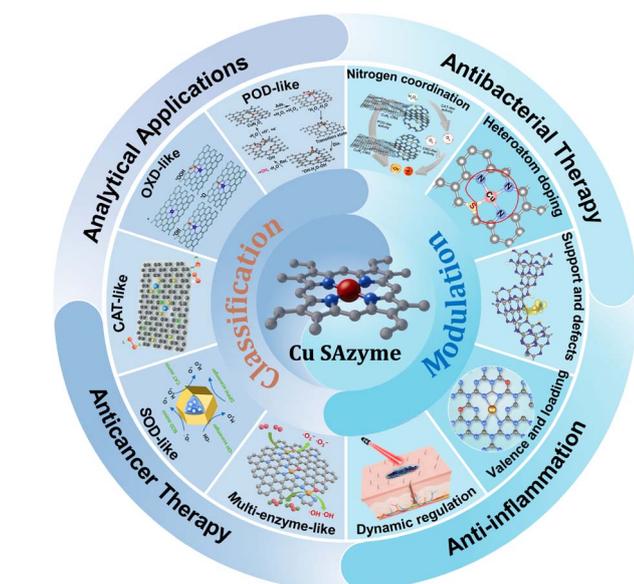

Fig. 1 A schematic overview of the enzyme-like properties, modulation strategies, and major applications of Cu SAzymes.
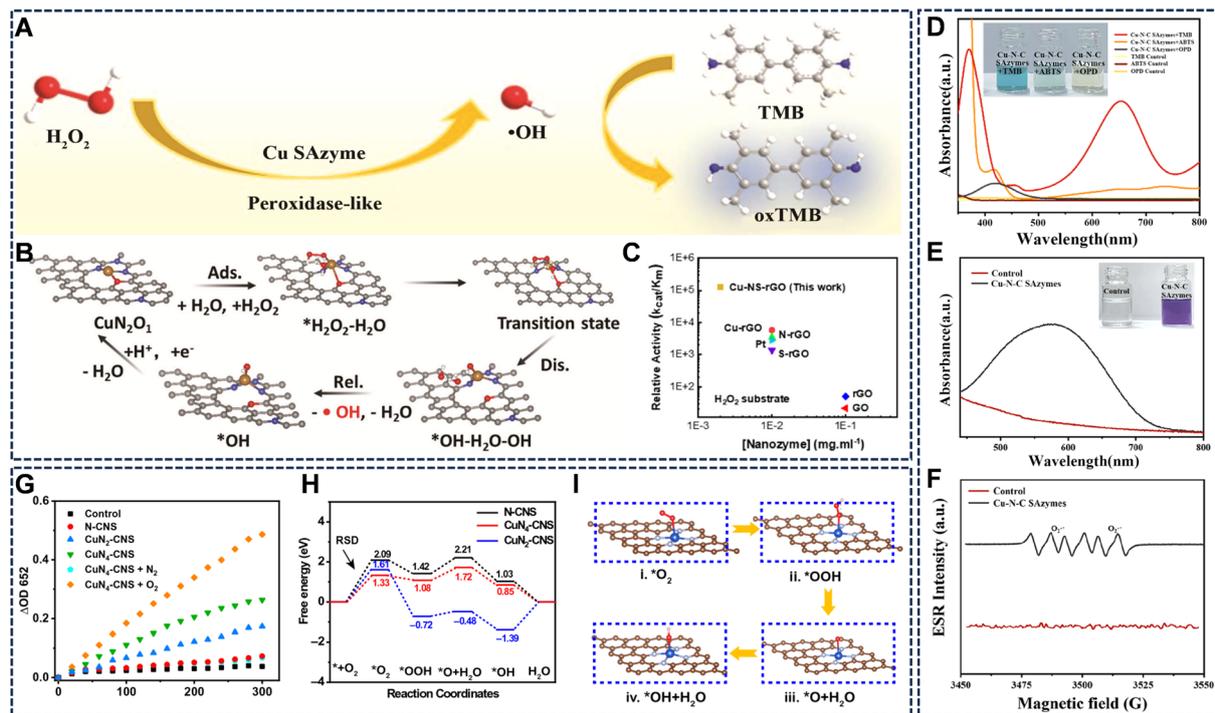
Fig. 2 (A and B) The POD-like catalytic mechanism of Cu SAzymes. Reproduced with permission from ref. 36 and 37 Copyright (2023) Wiley-VCH. (C) The outstanding catalytic performance of Cu-N$_4$/S-rGO. Reproduced with permission from ref. 39 Copyright (2024) Elsevier. (D) ABTS, TMB, and OPD catalyzed by Cu-N-C. Reproduced with permission from ref. 41 Copyright (2022) American Chemical Society. (E) UV-vis spectra of Cu-N-C in the NBT reaction system and (F) ESR spectra of O$_2$$^{\cdot-}$ produced by the DMPO-Cu-N-C. Reproduced with permission from ref. 41 Copyright (2022) American Chemical Society. (G) OXD-like activity of N-CNS, CuN$_2$-CNS, and CuN$_4$-CNS. Reproduced with permission from ref. 42 Copyright (2023) Science and Technology Review Publishing House. (H) OXD-like free energy diagram and (I) schematic representation of the catalytic reaction pathway. Reproduced with permission from ref. 42 Copyright (2023) Science and Technology Review Publishing House.

2.2.1 General OXD-like activity. Cu SAzymes demonstrate efficient OXD-like activity, catalyzing the oxidation of typical chromogenic substrates such as TMB, OPD, and ABTS in the presence of O$_2$ (Fig. 2D).[17,41,42] This process mimics natural oxidases by activating O$_2$ and facilitating electron transfer. Experimental and theoretical studies reveal that atomically dispersed Cu sites promote the reduction of O$_2$ to superoxide anions (O$_2$$^{\cdot-}$), which subsequently participate in substrate oxidation. ESR analyses using 5,5-dimethyl-1-pyrroline N-oxide (DMPO) as a spin trap have confirmed the generation of O$_2$$^{\cdot-}$ during catalytic reactions (Fig. 2E and F).[17,41]
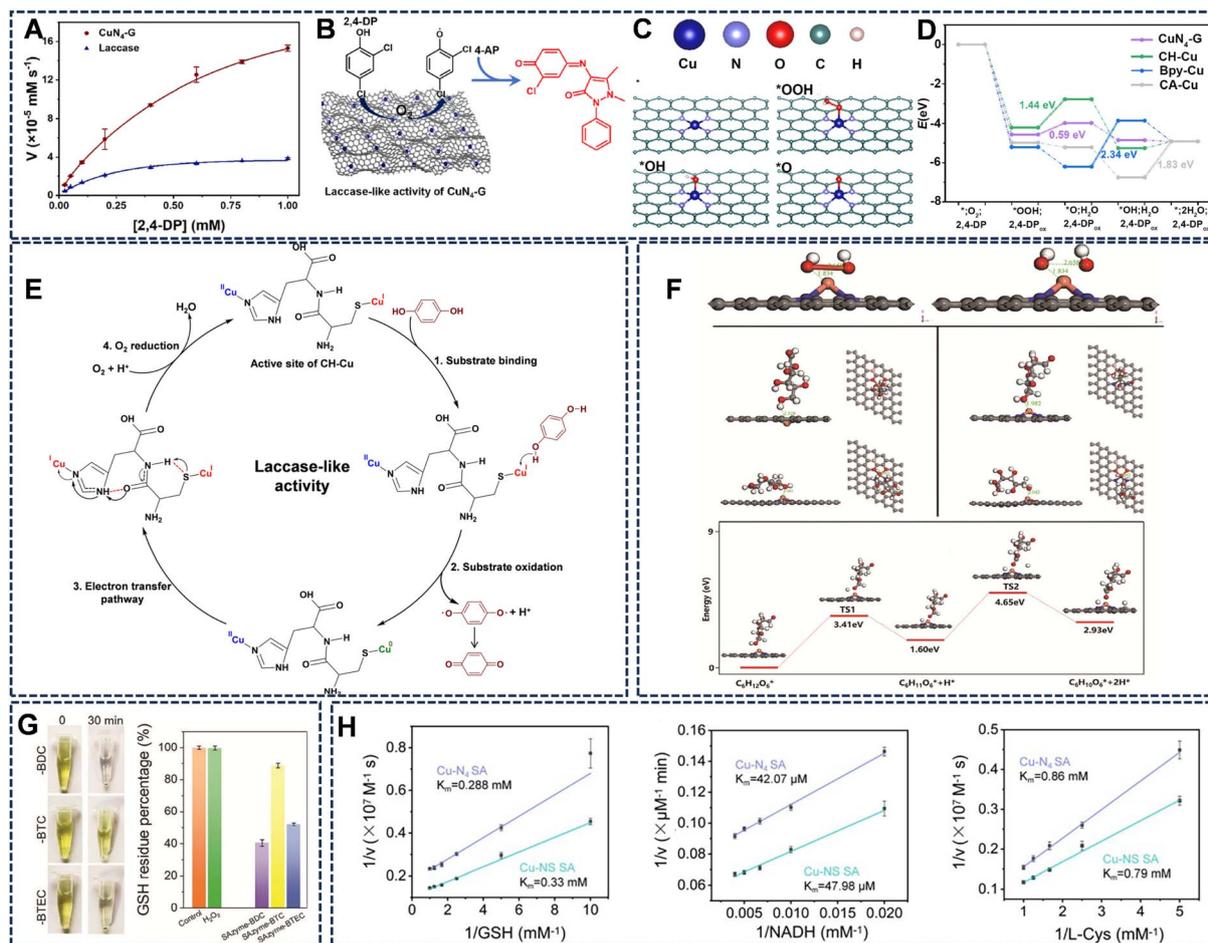
The OXD-like activity of Cu SAzymes is closely related to their electronic structure and local coordination environment. For instance, Cu-N$_4$ configurations exhibit a superior catalytic performance compared to Cu-N$_2$ sites, as evidenced by lower O$_2$ reduction rates (Fig. 2G).[42] DFT calculations have revealed that the Cu-N$_4$ coordination structure possesses an optimal O$_2$ adsorption energy and a low reaction barrier for catalytic oxidation, outperforming Cu-N$_2$ sites in both adsorption and electron-transfer efficiency (Fig. 2H and I). The catalytic process involves the reversible redox cycling of Cu between Cu(I) and Cu(II) oxidation states, resembling the catalytic behavior of natural copper-containing oxidases. The N-doped carbon support facilitates charge delocalization and provides strong π-d orbital coupling between Cu centers and the carbon

framework, thus promoting efficient electron transfer to O$_2$ and facilitating ROS formation.

2.2.2 Laccase-like activity. Laccases are copper-containing enzymes that catalyze the oxidation of phenolic compounds while reducing O$_2$ to H$_2$O. Cu SAzymes can mimic this activity, offering enhanced stability and tunability. For instance, CuN$_4$ anchored on nitrogen-doped graphene (CuN$_4$-G) demonstrates exceptional laccase-like activity, efficiently oxidizing phenolic substrates across a wide range of pH, temperature, and ionic strength conditions (Fig. 3A and B).[43] Similarly, CH-Cu, a nanozyme synthesized via coordination of Cu(I)/Cu(II) with a cysteine–histidine dipeptide, showed a comparable K_m value but higher V_{max} than laccase, alongside excellent recyclability and substrate universality.[44]

The catalytic mechanism of laccase-mimicking copper nanozymes involves the oxidation of phenolic compounds coupled with the four-electron reduction of O$_2$ to water, bypassing the generation of H$_2$O$_2$. DFT calculations indicate that the electron coupling effect in the Cu-N$_4$ structure facilitates rapid electron transfer and enhances electrical conductivity, leading to a lower energy barrier in the rate-determining step (Fig. 3C and D).[43] In the case of the cysteine (Cys)–histidine (His) dipeptide coordinated Cu(I)/Cu(II) (CH-Cu), the proposed mechanism involves substrate oxidation near Cu$^+$ sites, electron transfer via the Cys–His pathway, and O$_2$ reduction at Cu^{2+} sites,

Fig. 3 (A and B) CuN$_4$-G exhibits outstanding catalytic performance in the oxidation reaction of phenolic substrates and the reaction of 2,4-DP and 4-AP catalyzed by CuN$_4$-G. (C and D) The intermediate structures of surface O species on the CuN$_4$-G, and the free energy diagram of 2,4-DP oxidation reaction pathways on the surface of four catalytic models. Reproduced with permission from ref. 43 Copyright (2023) Elsevier. (E) Schematic of possible catalytic mechanism involving the CH-Cu nanozymes (black dotted lines indicate through-space interactions and red dotted lines indicate H-bonds). Reproduced with permission from ref. 44 Copyright (2022) Elsevier. (F) DFT calculations were employed to predict and evaluate POD-like and GAO-like reactions. Reproduced with permission from ref. 45 Copyright (2024) Wiley-VCH. (G) Cu SAzyme exhibits both GSHOx and GPx activities, demonstrating optimal performance. Reproduced with permission from ref. 46 Copyright (2024) Wiley-VCH. (H) Comparative kinetic studies indicate that Cu-N$_3$S$_1$ exhibits superior substrate affinity and electron transfer properties. Reproduced with permission from ref. 19 Copyright (2023) Wiley-VCH.

closely resembling the electron transfer pathway in natural laccase (Fig. 3E).[44] This biomimetic approach ensures efficient catalytic cycles without the instability associated with natural enzymes.

2.2.3 GAO-like activity. Cu SAzymes exhibit GAO-like activity, selectively oxidizing D-galactose and other primary alcohols to corresponding aldehydes while generating H$_2$O$_2$ as a byproduct.[45] This activity showcases high stereospecificity, with preferential oxidation of D-galactose and structurally similar compounds like D-galactosamine and dihydroxyacetone, while remaining inactive toward L-galactose or unrelated carbohydrates such as glucose and fructose. DFT calculations reveal that the adsorption energy of D-galactose on the Cu-SAN surface is significantly stronger than that of L-galactose, due to favorable interactions between the Cu atom and oxygen atoms in the D-galactose (Fig. 3F). The proposed catalytic cycle

involves the activation of O$_2$ at the Cu center, followed by hydrogen abstraction from the substrate, leading to aldehyde formation and H$_2$O$_2$ release.

2.2.4 Other specific OXD-like activities. Cu SAzymes also demonstrate versatile OXD-like activities toward specific reducing substrates, including GSHOx, LCO, and NOx.[19,46] For instance, Cu SAzymes exhibit GSHOx-like activity through their atomically dispersed coordination centers, catalyzing the oxidation of GSH to GSSG, accompanied by the generation of H$_2$O$_2$.[46] Cu SAzymes also catalyze rapid GSH oxidation, as shown by DTNB-based colorimetric assays, with SAzyme-BDC displaying the highest activity (Fig. 3G). The presence of low concentrations of H$_2$O$_2$ further accelerates GSH depletion, indicating synergistic GSHOx- and GSH peroxidase (GPx)-like activities. DFT simulations revealed that GSH oxidation occurs *via* stepwise adsorption and activation on Cu-N$_4$ sites with low

Gibbs free energy barriers, demonstrating the intrinsic efficiency of these single-atom centers. Similarly, the NOx-like pathway oxidizes NADH to NAD$^+$ while the LCO-like pathway oxidizes L-cysteine to cystine using O_2 as the electron acceptor (Fig. 3H).[19]

In summary, the OXD-like activities of Cu SAzymes span general substrate oxidation and highly specific reactions. Continued exploration of these activities will further unlock their potential in biotechnology and medicine.

2.3 CAT-like activity

Cu SAzymes have emerged as potent CAT mimics, efficiently catalyzing the decomposition of H_2O_2 into O_2 and water (H_2O). Compared to natural CAT, Cu SAzymes offer enhanced stability, tunable coordination structures, and responsiveness to external stimuli, making them versatile O_2-generating catalysts.[42,47–50] The CAT-like reaction pathway initiates with H_2O_2 adsorption at isolated copper centers, followed by O–O bond weakening and subsequent O_2 release. Spectroscopic analyses and DFT calculations highlight the coordination environment as the determinant of CAT-like performance.

Systems such as CuN$_4$-CNS can generate substantial amounts of O_2 rapidly, rivaling the performance of classical CAT

mimics like Pt/C (Fig. 4A).[42] This O_2-generation capability is crucial for modulating hypoxic environments, particularly in tumor therapy. Furthermore, the CAT-like activity can be integrated with other functions. For example, L-Arg@Cu-SAzymes not only possessed CAT-like activity to generate O_2 but also could efficiently load L-arginine to mediate NO release, triggering subsequent reactive nitrogen species generation (Fig. 4B).[51]

2.4 SOD-like activity

SOD-like activity is a critical feature of Cu SAzymes, enabling them to catalyze the dismutation of $O_2^{•-}$ into H_2O_2 and O_2, thereby intercepting ROS and mitigating oxidative damage. While POD- and CAT-like activities have been extensively studied, reports on SOD-like catalysis remain limited due to challenges in selectively converting $O_2^{•-}$ while maintaining catalytic stability.

For instance, a de novo-designed Cu-N$_4$ SAzyme successfully reproduced the electronic and structural features of Cu-SOD5, exhibiting strong and stable $O_2^{•-}$ dismutation activity across a wide pH range (1–13) and temperature range (4–90 °C), surpassing the stability of natural SOD (Fig. 4C).[52] Notably, graphene oxide (GO)-supported Cu single-atom catalysts (Cu/
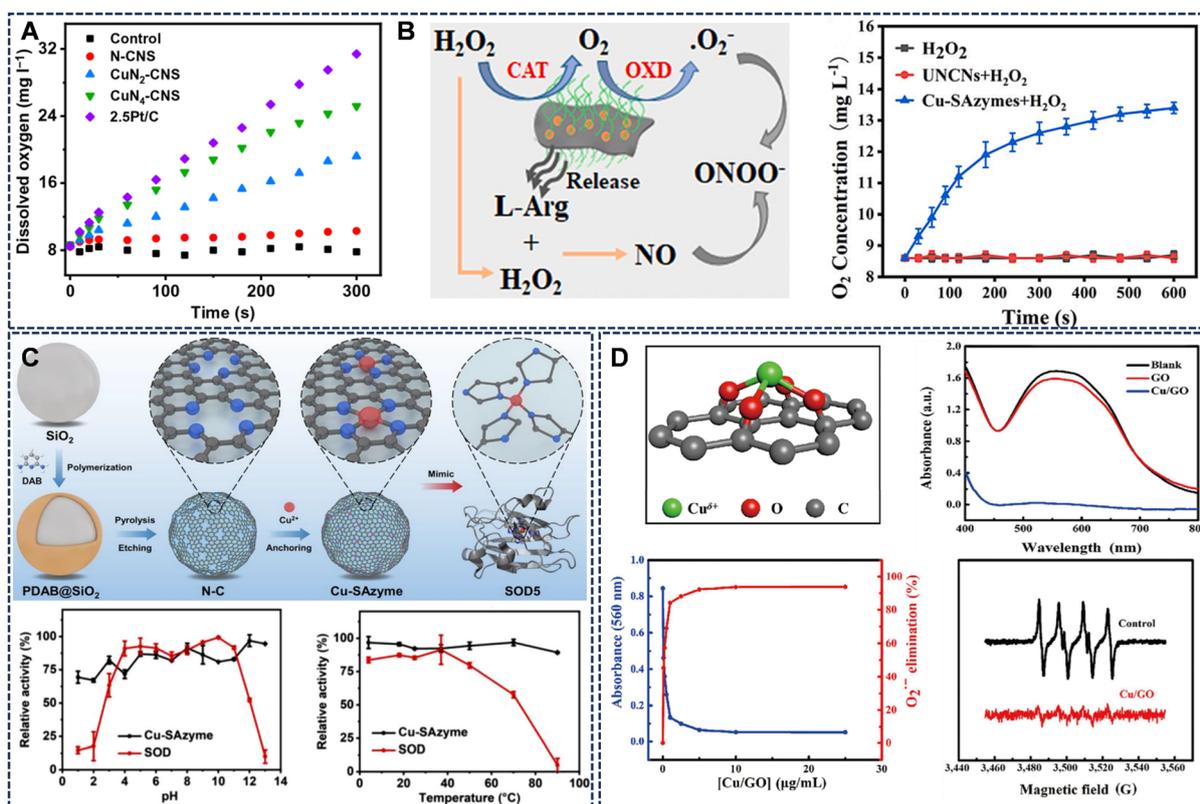

Fig. 4 (A) CuN$_4$-CNS rivals the O_2 evolution capacity of the classic CAT simulant Pt/C. Reproduced with permission from ref. 42 Copyright (2023) Science and Technology Review Publishing House. (B) L-Arg@Cu-SAzymes not only possessed CAT- and OXD-like activities to generate cytotoxic $O_2^{•-}$, but also can efficiently load L-arginine to mediate NO release and trigger subsequent ONOO generation. Reproduced with permission from ref. 51 Copyright (2023) Elsevier. (C) Synthesis schematic illustration of Cu-SAzyme and its potent and stable SOD-like enzyme activity across a broad pH range (1–13) and temperature range (4–90 °C). Reproduced with permission from ref. 52 Copyright (2022) John Wiley and Sons. (D) The possible coordination structure of Cu/GO SACs material and its excellent SOD-like properties. Reproduced with permission from ref. 53 Copyright (2022) Springer Nature.

GO SACs) exhibit exceptional specificity for $O_2^{\cdot-}$ dismutation without engaging in Fenton-like or POD side reactions (Fig. 4D).[53] This selectivity arises from atomic-level coordination sites, which create an electronic environment favoring $O_2^{\cdot-}$ binding and redox cycling. ESR spectra and nitroblue tetrazolium (NBT) inhibition assays confirm efficient $O_2^{\cdot-}$ elimination and concentration-dependent SOD-like responses.

2.5 Multi-enzyme-like activities

Unlike natural enzymes that typically exhibit singular catalytic specificity evolved for precise biological functions, Cu SAzymes demonstrate remarkable multi-enzyme mimicking capabilities that enable complex cascade reactions reminiscent of natural enzymatic systems. This unique characteristic stems from their tunable atomic coordination environments and versatile redox chemistry, allowing simultaneous or switchable expression of POD-, CAT-, OXD-, and SOD-like activities under physiological conditions.

The multi-enzyme functionality enables sophisticated therapeutic applications through synergistic effects. For example, CuN_4-CNS SAzyme exhibited triple enzyme-like activities (POD-, CAT-, and OXD-like), facilitating parallel and cascaded reactions for ROS generation. Particularly noteworthy is its exceptional CAT-like activity that decomposes H_2O_2 into O_2,

subsequently utilized by OXD-like activity to generate $O_2^{\cdot-}$, creating self-supplying catalytic cycles in hypoxic environments. In another work, Cu-N,O/C nanozymes exhibit concurrent POD-like activity for $\cdot OH$ generation, CAT-like activity for O_2 production, and OXD-like activity for $O_2^{\cdot-}$ formation, effectively creating ROS storms in tumor microenvironments.[54] This coordinated action addresses multiple therapeutic barriers simultaneously: CAT-like activity alleviates hypoxia, while POD- and OXD-like activities synergize to enhance oxidative stress.

In summary, the multi-enzyme capabilities of Cu SAzymes represent a paradigm shift in artificial enzyme design, moving beyond single-activity mimicry to integrated catalytic systems. Through precise coordination engineering, these nanomaterials achieve sophisticated reaction control that addresses complex biological challenges, positioning them as powerful tools for next-generation biomedical applications.

3. Strategies for modulating the catalytic activity

The catalytic properties of Cu SAzymes are intricately linked to the specific coordination environment of the copper centers, and the relationship between these parameters and the enzyme-like functions is summarized in Table 1. These diverse enzyme-

Table 1 Coordination environment parameters and enzyme-like catalytic reactions of materials

Nanozyme	Active center	Supporting materials	Enzyme-like activity	Substrates	K_m (mM)	V_{max} (M min^{-1})	k_{cat} (min^{-1})	Ref.
CuSACO	Cu-C$_3$	Graphene	POD-like	H$_2$O$_2$	4.87	7.5×10^{-4}	0.96	48
			CAT-like	H$_2$O$_2$	12.48	1.2×10^{-3}	1.54	
			OXD-like	TMB	0.13	1.74×10^{-6}	1.54	
CuN$_3$-SAzyme	Cu-N$_3$	2D carbon nanosheets	POD-like	H$_2$O$_2$	65.8	8.76×10^{-5}	9.41	55
				TMB	1.61	9.84×10^{-5}	10.57	
CuN$_4$-SAzyme	Cu-N$_4$			H$_2$O$_2$	752	4.80×10^{-6}	1.27	
				TMB	14.2	7.8×10^{-6}	2.06	
Cu-CNNDs	Cu-N$_3$	Atomic-thick C$_3$N$_4$	POD-like	H$_2$O$_2$	1.26	4.61×10^{-6}	17.0	36
				TMB	0.186	3.61×10^{-6}	13.25	
CuN$_4$-CNS	Cu-N$_4$	N-doped carbon nanosheets	POD-like	H$_2$O$_2$	5.63	8.28×10^{-5}	N.D.	42
				TMB	0.22	5.7×10^{-6}	N.D.	
			OXD-like	TMB	0.57	3.9×10^{-6}	N.D.	
Cu SAs/CN	Cu-N$_4$	g-C$_3$N$_4$	APX-like	AsA	0.01	1.15×10^{-5}	2.67	56
Cu-N/S-C	Cu-N$_1$S$_2$	N-doped carbon	CAT-like	H$_2$O$_2$	13.32	1.86×10^{-4}	311.4	18
			POD-like	H$_2$O$_2$	15.41	8.08×10^{-5}	13.8	
Cu-N-C	Cu-N$_3$		CAT-like	H$_2$O$_2$	183.9	1.72×10^{-4}	66.0	
			POD-like	H$_2$O$_2$	22.60	4.42×10^{-5}	6.6	
Cu-NS-rGO	Cu-N$_4$S	rGO	POD-like	H$_2$O$_2$	3.122	N.D.	N.D.	39
				TMB	0.078	N.D.	N.D.	
Cu-NS@UK@POx	Cu-N$_3$S$_1$	N-doped carbon	POD-like	H$_2$O$_2$	0.45	9.96×10^{-6}	0.66	19
			NOx-like	NADH	0.048	1.81×10^{-5}	11.98	
			GSHOx-like	GSH	0.33	5.71×10^{-5}	37.8	
			LCO-like	L-Cys	0.79	9.20×10^{-5}	69.6	
Au@CuBCats	Cu-N$_2$O$_1$	N-doped carbon	POD-like	H$_2$O$_2$	1.789	3.4×10^{-5}	N.D.	37
Cu-N/O	Cu-N$_2$O$_2$	N-doped carbon	POD-like	H$_2$O$_2$	2.61	1.24×10^{-4}	134.4	16
				TMB	1.24	1.31×10^{-4}	100.8	
F@D-CHTP SN-MF	Cu-O$_2$	Cu-HTP MOFs	POD-like	TMB	3.47	8.4×10^{-6}	N.D.	57
ac-Cu-D	Cu-O$_2$	N-doped carbon	POD-like	H$_2$O$_2$	14.7	1.07×10^{-5}	N.D.	58
CuN-CDs	Cu-O$_4$	Lignosulfonate	OXD-like	TMB	0.17	4.9×10^{-6}	N.D.	59
			POD-like	TMB	0.18	2.41×10^{-5}	N.D.	

like activities of Cu SAzymes can be precisely programmed and dynamically regulated through rational design. This chapter systematically delineates the primary strategies for modulating catalytic performance, progressing from static structural engineering at the atomic level to dynamic control *via* external physical fields.

3.1 Role of nitrogen coordination number

The nitrogen coordination number in Cu SAzymes is a fundamental structural parameter that dictates the geometric configuration and electronic structure of the copper center, thereby exerting a profound influence on the type and efficiency of enzyme-mimicking reactions. By precisely tailoring the first coordination sphere (*e.g.*, Cu-N$_2$, Cu-N$_3$, Cu-N$_4$), the dynamic evolution and stability of the active site under operational conditions are equally critical for sustained therapeutic efficacy.[60]

In general, a lower coordination number often creates an unsaturated and electron-rich metal center, which favors the adsorption and activation of substrates. This is particularly beneficial for POD-like activity. For instance, Wu *et al.* demonstrated that Cu-N$_3$ configurations consistently demonstrate superior POD-like performance compared to their Cu-N$_4$ counterparts.[55] As highlighted in Fig. 5A, the CuN$_3$-SAzyme exhibits a specific POD activity of 11.33 U mg^{-1}, significantly surpassing that of Cu-N$_4$-based nanozymes (2.08 U mg^{-1}). Kinetic analyses further corroborate this advantage, with CuN$_3$-SAzyme showing a lower K_m of 0.658 mM for H$_2$O$_2$, indicating stronger substrate affinity. DFT calculations suggested that most of the Cu d-states in CuN$_3$-SAzyme lie within an energy range 2 eV below the Fermi level, whereas the vast majority of Cu d-states in CuN$_4$-Sazyme lie outside this range. Furthermore, the single Cu atom on CuN$_3$-SAzyme protrudes more than 2 Å above the graphene
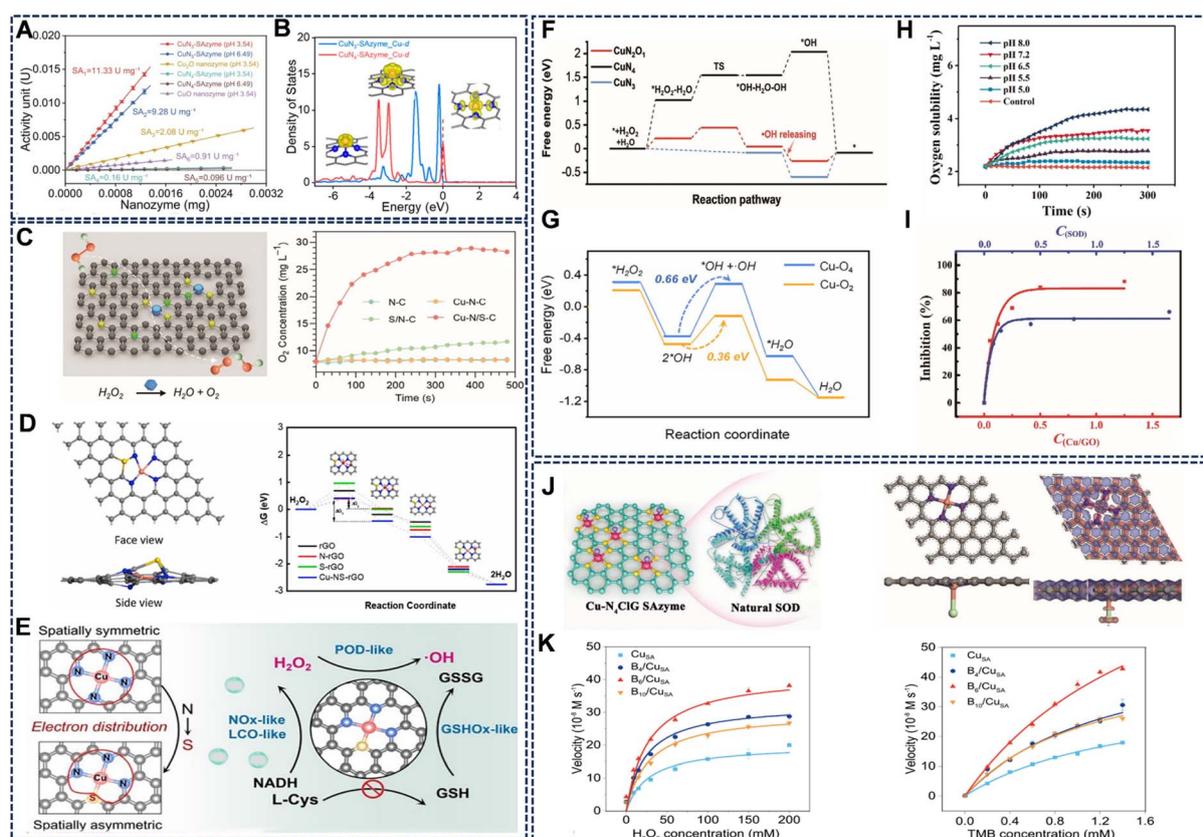

Fig. 5 (A) The POD activity of Cu-N$_3$-SAzyme is significantly higher than that of Cu-N$_4$-SAzyme, and (B) calculated density of states for the d-orbitals of Cu single atom on CuN$_3$-SAzyme and CuN$_4$-SAzyme. Reproduced with permission from ref. 55 Copyright (2024) Springer Nature. (C) The catalytic activity of the Cu-N/S-C system was enhanced by 65.2-fold compared to the Cu-N$_3$ site. Reproduced with permission from ref. 18 Copyright (2023) Wiley-VCH. (D) Structural simulation of Cu-N$_4$S active site-containing Cu-NS-rGO and outstanding POD-like catalytic activity. Reproduced with permission from ref. 39 Copyright (2024) Elsevier. (E) The introduction of S endows the Cu-N$_3$S$_1$ active site with strong electron transfer ability, which enhances the multi-enzyme activities of Cu-NS SA. Reproduced with permission from ref. 19 Copyright (2023) Wiley-VCH. (F) Free energy diagram for the reaction process on CuN$_2$O$_1$, CuN$_4$, and CuN$_3$ sites. Reproduced with permission from ref. 37 Copyright (2023) Wiley-VCH. (G) Corresponding free energy diagram for the POD-like reaction on Cu-O$_4$ and Cu-O$_2$ catalytic sites. Reproduced with permission from ref. 57 Copyright (2024) Elsevier. (H) PH-responsive POD-like behaviour. Reproduced with permission from ref. 58 Copyright (2024) Wiley-VCH. (I) The relationship between inhibition of NBT reduction by O$_2$$^{\cdot-}$, and concentration of Cu/GO SACs and natural SOD enzyme. Reproduced with permission from ref. 53 Copyright (2022) Springer Nature. (J) Schematic illustrations of Cu-N$_4$ClG SAzyme synthesis and the DFT calculation-rooted energy diagrams of the SOD-like catalytic reaction process. Reproduced with permission from ref. 63 Copyright (2022) Wiley-VCH. (K) Response of CuSA, B$_4$/CuSA, B$_6$/CuSA and B$_{10}$/CuSA to varying concentrations of H$_2$O$_2$ and TMB. Reproduced with permission from ref. 64 Copyright (2025) American Chemical Society.

plane, which facilitates the binding with H_2O_2 compared with the in-plane Cu atom on CuN_4-SAzyme.

In contrast, tetracoordinated Cu-N_4 centers, with their more symmetric and stable coordination geometry, often support a broader spectrum of enzyme-like activities and demonstrate higher performance in certain oxidation reactions. For example, Bai *et al.* compared CuN_2-CNS and CuN_4-CNS SAzymes, showing that increasing the coordination number from 2 to 4 enhances multi-enzyme performance (Fig. 5B).[42] Specifically, in OXD-like catalysis, the CuN_4-CNS SAzyme outperforms the CuN_2-CNS analogue, achieving a lower K_m (0.57 mM) for TMB, as detailed in Table 1. This is due to the optimal O_2 adsorption energy and facilitated electron transfer provided by the Cu-N_4 structure. Furthermore, the Cu-N_4 configuration is highly effective for mimicking antioxidant enzymes like ascorbate peroxidase (APX), with Cu SAs/CN nanozymes exhibiting a K_m for ascorbic acid as low as 0.01 mM, rivaling natural enzymes.[56]

In summary, the nitrogen coordination number serves as a powerful knob to tune catalytic specificity. Lower coordinations (*e.g.*, Cu-N_3) are preferred for maximizing POD-like activity due to unsaturation and high substrate affinity, while Cu-N_4 sites are often superior for multi-enzyme activities and certain OXD-like reactions, offering a balanced electronic structure that accommodates diverse catalytic cycles.

3.2 Effect of heteroatom doping

Beyond the nitrogen coordination number, introducing heteroatoms (*e.g.*, S, O, Cl, B) into the first coordination sphere of copper is a sophisticated strategy to break coordination symmetry, tailor the electronic structure, and thereby dramatically enhance catalytic performance. This approach allows for fine-tuning that surpasses the capabilities of pure Cu-N_x sites.

3.2.1. Sulfur doping. Sulfur doping is exceptionally effective in creating asymmetric coordination environments (*e.g.*, Cu-N_3S_1, Cu-N_1S_2), which induces an uneven distribution of electron density around the Cu center. This electronic asymmetry significantly improves substrate adsorption and reaction kinetics across multiple enzyme activities. For instance, the incorporation of S into a Cu-N_1S_2 site (Cu-N/S-C) resulted in a remarkable 13.8-fold increase in H_2O_2 affinity and a 65.2-fold boost in CAT-like efficiency compared to a Cu-N_3 site (Fig. 5C).[18] DFT calculations confirm that S-atom incorporation optimizes the geometric and electronic structure, lowering the energy barrier for H_2O_2 activation. Similarly, sulfur-doped Cu-NS-rGO nanozymes exhibit superior POD-like activity owing to the synergistic effect of Cu-N_4S sites in enhancing electron transfer (Fig. 5D).[39] Furthermore, the Cu-NS@UK@POx SAzymes (with Cu-N_3S_1 sites) exhibit broadened catalytic capabilities, including POD-, GSHOx-, NOx-, and LCO-like activities (Fig. 5E).[19] The asymmetric electron distribution in the Cu-N-S configuration lowers the energy barrier for O_2 adsorption and activation, thereby accelerating the oxidation kinetics of various substrates. Taking the POD-like property as an example, DFT calculations consistently show that Cu-NS SA binds H_2O_2 far more strongly (−0.42 eV *vs.* −0.05 eV on Cu-N_4 SA) and spontaneously splits it into two *OH ($\Delta G = -0.64$ eV), whereas Cu-N_4

SA faces a 0.59 eV barrier. The desorption of *OH to form free ·OH is the rate-limiting step, where the energy barrier of the Cu-NS SA (−0.34 eV) is significantly lower than that of the Cu-N_4 SA (0.72 eV), indicating that the Cu-NS SA favors the generation of ·OH. Thus, the introduction of sulfur endows the Cu-N_3S_1 active site with stronger electron transfer ability, which effectively optimizes the free energy of each step of the reaction and reduces the activation barrier of the rate-limiting step to accelerate the reaction.

3.2.2. Oxygen incorporation. Oxygen atoms incorporated into Cu-N coordination spheres fine-tune catalytic activity by altering charge distribution and stability. For instance, replacing a nitrogen atom with oxygen in the coordination sphere, as in the CuN_2O_1 site of Au@CuBCats, creates a highly efficient POD mimic.[37] DFT calculations reveal that this structure exhibits a lower energy barrier for H_2O_2 decomposition and ·OH desorption compared to CuN_4 and CuN_3 sites, facilitating efficient cascade catalysis for diabetic ulcer treatment (Fig. 5F). The optimized coordination geometry allows stronger H_2O_2 adsorption and faster electron transfer, leading to enhanced antibacterial efficacy against multidrug-resistant bacteria. In Cu-N/O SAzymes with Cu-N_2O_2 coordination, oxygen doping further improves POD-like activity and photothermal conversion efficiency.[16] These sites show a K_m of 2.61 mM for H_2O_2 and 1.24 mM for TMB, outperforming pure Cu-N_4 centers due to improved electron excitation from electrophilic oxygen atoms. The construction of an asymmetric CuN_3O coordination environment can more profoundly modulate the electronic structure of copper centers.[61] This asymmetric configuration induces an uneven electron distribution around the Cu center, significantly enhancing O_2 activation and substrate oxidation kinetics. Such structural features endow CuN_3O-based SAzymes with markedly improved catechol oxidase (CO)-like and OXD-like activity by lowering the reaction barrier for O_2 reduction and accelerating the electron-transfer process. These findings highlight that introducing a single oxygen atom into a Cu-N_x framework offers a more efficient strategy to break symmetry, optimize charge redistribution, and enhance multi-enzyme catalytic functions compared with conventional Cu-N_x sites.

3.2.3. Direct oxygen coordination. Direct bonding between copper and oxygen ligands can unlock unique catalytic mechanisms and biological functions. For instance, exposed Cu-O_2 sites in F@D-CHTP SN-MF nanozymes favor POD-like activity and have been shown to trigger cuproptosis by promoting mitochondrial dysfunction (Fig. 5G).[57] This configuration also stabilizes transition states for O_2 reduction, leading to synergistic CAT-like and SOD-like activities in tumor therapy. Similarly, ac-Cu-D SAzymes with Cu-O_2 centers exhibit pH-responsive POD-like behavior, with a K_m of 14.7 mM for H_2O_2, and leverage photothermal effects for anaerobic glycolysis interference (Fig. 5H).[58] Cu-O_4 coordination in graphene oxide (Cu/GO SACs) creates an electronic environment that favors superoxide dismutation, conferring highly specific SOD-like activity without engaging in Fenton-like side reactions (Fig. 5I).[53] DFT analyses indicate that oxygen incorporation strengthens Cu-O interactions, reducing the activation energy for substrate dissociation and enhancing catalytic durability

under physiological conditions. Differently, $Cu-O_4$ coordinated in lignin polyphenol network (Cu-SLCDs) exhibit enhanced multienzyme-like (OXD-, POD-, SOD-, and CAT-like) activities.[62] Experiments and theoretical calculations demonstrate that the polyphenol p-π conjugated structure creates a unique electron-donating coordination environment, which increases the electron density of Cu-SLCDs at the Fermi level, enhances electron transfer, and boosts multienzyme-like activities.

3.2.4. Axial ligation. Introducing heteroatoms in the axial position of the copper center introduces steric and electronic effects that can refine catalytic specificity. In the $Cu-N_4ClG$ SAzyme, an axial chlorine ligand fine-tunes the geometric and electronic structure to closely mimic natural SOD (Fig. 5J).[63] This $Cl-Cu-N_4$ configuration optimizes orbital overlap with reactive oxygen intermediates, resulting in highly efficient and sequential SOD-/CAT-like activities for treating osteoarthritis. In another work, Hu et al. demonstrated that the incorporation of B-O sites into single-atom Cu-N catalysts (B_6/Cu_{SA}) polarizes the Cu centers via electron redistribution, which accelerates H_2O_2 adsorption and O–O bond cleavage.[64] This electronic modulation lowers the Michaelis constant and doubles the maximal velocity, delivering a three-fold enhancement in POD-like activity (Fig. 5K).

In conclusion, heteroatom doping is a versatile and powerful tool for engineering the catalytic properties of Cu SAzymes. By carefully selecting the dopant atom and its position within the coordination sphere, it is possible to selectively enhance specific enzyme-like activities, introduce multi-functionality, and achieve unprecedented levels of catalytic selectivity for advanced biomedical applications.

3.3 Support structures and defects

The support material of Cu-SAzymes is not merely an inert scaffold but also plays an active role in stabilizing single copper atoms and modulating the catalytic performance through its structure, composition, and defects.

3.3.1. Support types. Extensive research has identified several categories of high-performance supports, each with distinct advantages. Carbon-based materials, particularly nitrogen-doped carbon (N-C) derived from metal–organic frameworks (MOFs) or polymers, are widely used due to their high surface area, rich pore structure, and strong metal-nitrogen (M−N) coordination sites that prevent aggregation.[18,52] For instance, N-C supports synthesized from 2,6-diaminopyridine pyrolysis exhibit a large surface area (985 $m^2 g^{-1}$) and abundant pyridinic N species, which serve as robust anchoring sites for Cu^{2+} cations, creating a well-defined micro-environment.[52] Two-dimensional (2D) materials, such as graphene, reduced graphene oxide (rGO), and MXenes, offer an ultra-large specific surface area and tunable electronic structures.[48,53,65] Their abundant surface functional groups and metal-vacancy defects make them ideal substrates for anchoring single atoms. Metal oxides, such as MoO_x, are versatile substrates due to their abundant and adjustable surface defects (e.g., oxygen vacancies), which act as stable sites for single-atom metals.[66]

Furthermore, the electronic structure and coordination environment provided by different supports critically determine the catalytic behavior of Cu SAzymes. For instance, a comparative theoretical-experimental investigation demonstrated that Cu single atoms dispersed on $g-C_3N_5$ form a well-defined Cu-N coordination environment, in which the unique pentazine-based structure strengthens Cu anchoring and facilitates charge redistribution between the metal center and the support (Fig. 6A and B).[60] This optimized electron density around Cu not only lowers the energy barrier of the rate-determining step in laccase-like reactions but also enhances substrate adsorption and electron-transfer efficiency. In contrast, supports such as $g-C_3N_4$ or C_3N_6 provide relatively weaker metal-support interactions, resulting in less favorable electronic modulation and inferior catalytic performance. The strengthened Cu-support interaction within $g-C_3N_5$ also suppresses atom aggregation, maintaining atomic dispersion during catalytic cycles and ensuring significantly higher laccase-like activity compared with Cu nanoparticles on the same substrate. These findings underline that tailoring the nitrogen configuration and electronic structure of carbon nitride supports is an effective strategy to boost Cu-based single-atom enzyme-mimicking activity.

3.3.2. Defect engineering. Beyond the intrinsic properties of the support, deliberate defect engineering has emerged as a powerful strategy to create abundant anchoring sites and modulate the electronic structure of the single-atom centers. The introduction of defects, such as nitrogen vacancies, dislocations, and edges, can significantly enhance catalytic efficiency by serving as traps for metal atoms and promoting charge carrier separation. Raman spectroscopy is a key tool for characterizing defect density, often revealed by a high intensity ratio of the D to G bands (I_D/I_G). For example, CuN_4-CNS nanozymes exhibit an I_D/I_G ratio of 0.99, indicating an abundance of defect sites originating from their porous structure and heteroatom doping, which correlates with high catalytic activity.[42]

3.3.3. Spatial and morphological control. The precise location of Cu atoms within a support and the overall morphology of the material significantly impact performance. For instance, confining Cu atoms in the interlayer of a polymer versus on the surface can lead to superior charge separation and substrate accessibility (Fig. 6C).[67] Similarly, constructing supports with hollow or wrinkled nanostructures maximizes the exposure of active sites and facilitates mass transfer, which is crucial for achieving high activity in complex biological environments.[68,69]

In conclusion, conductive or π-conjugated supports (e.g., graphene, carbon nitride) promote electron transfer, enhancing overall catalytic kinetics. Atomic dispersion stability and support interactions determine long-term durability and catalytic reproducibility, with strong metal-support coordination preventing Cu migration and maintaining single-atom integrity under physiological conditions.

3.4 Copper valence state and loading

The copper valence state and its loading amount are two interdependent parameters that directly influence the redox activity and the density of active sites.

3.4.1. Valence state. The mixed-valence Cu species (typically Cu(I)/Cu(II)) or a predominant Cu(I) state is often associated with
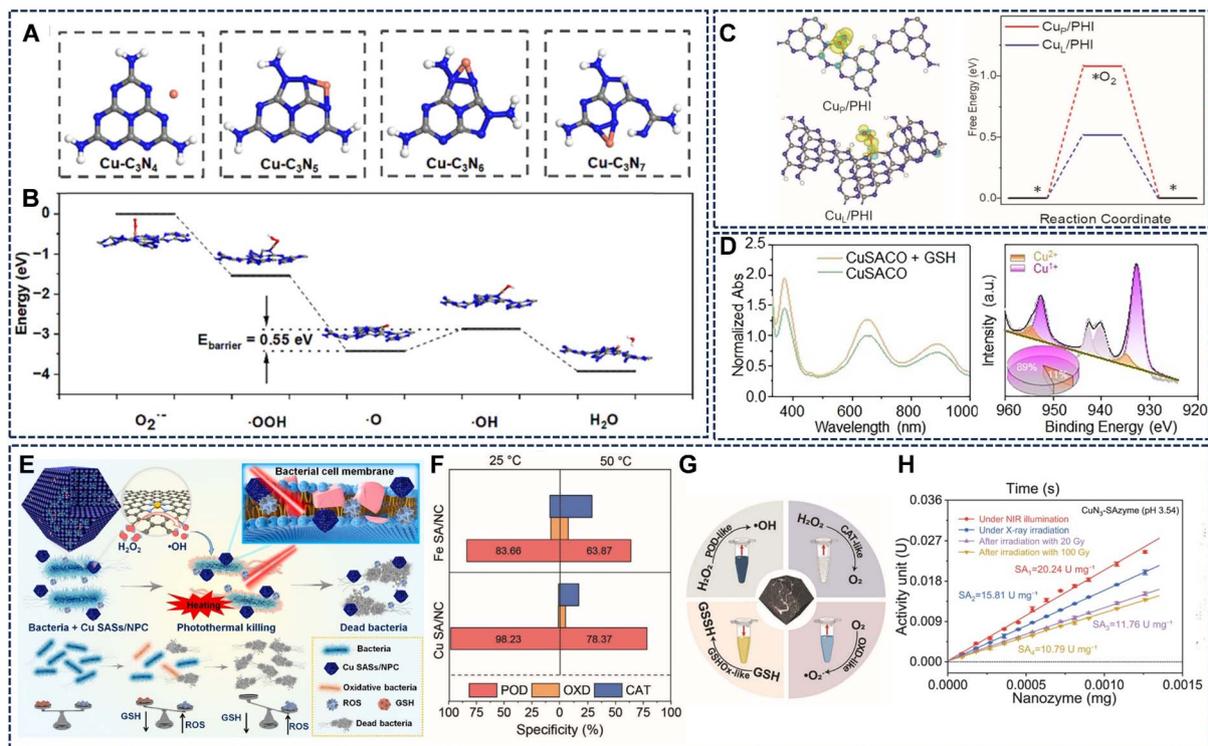
Fig. 6 (A) Schematic structure of g-C_3N_4, g-C_3N_5, C_3N_6, and C_3N_7 with Cu atoms, respectively. (B) Schematic calculation of the pathway of laccase activity of Cu SAs loaded on C_3N_5. Reproduced with permission from ref. 60 Copyright (2025) the Royal Society of Chemistry. (C) The charge density difference of the CuL/PHI and CuP/PHI with the adsorption of O_2 and DFT calculation of free energy of O_2 adsorption (ΔG^*O_2). Reproduced with permission from ref. 67 Copyright (2023) Wiley-VCH. (D) The dynamic interconversion between Cu^+ and Cu^{2+} driven by GSH. Reproduced with permission from ref. 48 Copyright (2024) Wiley-VCH. (E) Cu SASs/NPC with GSH-depleting performance were successfully synthesized for photothermal-catalytic therapy against bacteria. Reproduced with permission from ref. 71 Copyright (2021) Elsevier. (F) Photothermal effect-induced specific switching of enzyme activity in Cu SA/NC nanoenzymes. Reproduced with permission from ref. 47 Copyright (2023) Wiley-VCH. (G) Schematic diagram of the catalytic reaction of the multiple enzyme-like activities of Cu-NC. Reproduced with permission from ref. 72 Copyright (2023) Wiley-VCH. (H) CuN_3-SAzyme exhibits significantly enhanced POD-like activity under X-ray irradiation. Reproduced with permission from ref. 55 Copyright (2024) Springer Nature.

superior catalytic performance in various enzyme-mimicking reactions. For instance, Wu *et al.* identified that Cu(I) is more active for H_2O_2 activation in POD-like reactions and for sustaining catalytic cycles through dynamic Cu(I)/Cu(II) interconversion, driven by biological reductants such as GSH (Fig. 6D).[48] Beyond this specific interaction, strategies to stabilize the Cu(I) state, such as specific molecular coordination (*e.g.*, with L-cysteine) or *in situ* reduction in the tumor microenvironment, are key to maintaining high activity in physiological settings.[66]

3.4.2. Loading amount. While a high density of active sites is desirable, there exists an optimal loading amount. Excessive loading often leads to the aggregation of single atoms into nanoparticles, diminishing the unique catalytic properties of the single-atom sites. While ultrahigh Cu loadings up to 14.3 wt% and 23.36 wt% have been achieved on carbon nitride supports through specific synthetic routes that provide uniform and abundant anchoring sites,[69,70] there is often an optimal value for maximum catalytic efficiency. For instance, in MoO_x-Cu-Cys-PVP (MCCP) SAzymes, the Cu loading could be modulated from 1.59 to 26.67 wt%.[66] It was found that a loading of 10.10 wt% yielded the best CAT-like catalytic effect, whereas the higher loading of 26.67 wt% led to a reduction in activity due to the probable loss of

single-atom function. Thus, achieving the highest possible loading while maintaining perfect atomic dispersion is crucial for maximizing the atom utilization efficiency.

3.5 Dynamic regulation by external stimuli

Beyond static structural design, the catalytic activity of Cu SAzymes can be regulated dynamically and spatiotemporally by external physical stimuli, enabling on-demand therapy with high precision.

3.5.1. Photothermal stimulation. Light stimulation, particularly in the near-infrared (NIR) regions, serves as a predominant remote control modality due to its non-invasiveness and deep tissue penetration. Typically, NIR irradiation can significantly enhance the POD-like activity of Cu SASs/NPC by boosting the generation of hydroxyl radicals (Fig. 6E).[71] Furthermore, the spatial position of Cu atoms within a photosensitive support can be engineered to maximize photoinduced charge separation, drastically enhancing photocatalytic ROS generation for antibacterial applications.[67] Interestingly, the photothermal effect can even induce a switch in enzymatic specificity as well as accelerate the reaction kinetics. For instance, under NIR photothermal heating, Cu SA/NC nanoenzymes switch from predominant

POD-like activity at room temperature to additional OXD- and CAT-like activities, enabling an integrated pretreatment-and-sensing platform (Fig. 6F).[47]

3.5.2. Electric field stimulation. The utilization of an electric field, even a self-driven electric field generated by a tribo-electric nanogenerator (TENG), can universally enhance the multiple enzyme-like activities of a Cu SAzyme (Cu-NC).[72] Under an optimal AC electric field (20 V, 3 Hz), the POD, CAT, OXD, and GSHOx-like activities of Cu-NC were all significantly improved (Fig. 6G). The electric field facilitates substrate adsorption and alters the electron density of the Cu d-orbitals, thereby enhancing the overall catalytic kinetics. This opens avenues for self-powered, wearable device-modulated therapy.

3.5.3. Radiation stimulation. X-rays have also been applied for enhancing the enzyme-mimic activity of radioresistant Cu SAzymes. Notably, the POD-like activity of CuN_3-SAzyme was significantly enhanced upon X-ray exposure, attributed to the radiation-accelerated Cu^+/Cu^{2+} conversion cycle, which promotes catalytic kinetics (Fig. 6H).[55] This combination of inherent radioresistance and radiation-enhanced catalysis makes Cu-SAzymes excellent candidates for augmenting radiotherapy.

In summary, the catalytic performance of Cu SAzymes can be hierarchically modulated through an integrated design strategy that bridges static atomic architecture with dynamic responsiveness. The foundational approach involves atomic-level coordination environment (type/number of ligands, support) engineering to define the intrinsic activity and selectivity, establishing the core structure-activity relationship. This is synergistically enhanced by optimizing the copper valence state and loading amount, which can further optimize the electron transfer capability and the density of active sites, respectively, thereby amplifying the catalytic efficiency predefined by the atomic structure. Ultimately, external physical stimuli (light, electric fields, or radiation) can be coupled with the pre-designed nanozymes to achieve dynamic, spatiotemporal control over the catalytic activity, enabling stimulus-responsive on/off or enhanced functions in complex biological environments. This progressive optimization design logic provides a clear roadmap for the rational development of smart, next-generation nanozymes for precision biomedical applications.

4. Biosensing applications

Leveraging the tunable enzyme-like activities, high catalytic efficiency, and structural robustness, Cu SAzymes have become powerful tools in analytical chemistry. The integration into various sensing platforms has enabled the detection of a diverse range of analytes, from small molecules and ions to enzymes and entire cells. The following sections summarize these advances, categorized by detection modality, with a focus on application paradigms and performance metrics.

4.1 Colorimetric sensing

Colorimetric sensing, owing to its simplicity, low cost, and visual readout, is a dominant application for Cu SAzymes.[73,74]

Their OXD- and POD-like activities are particularly exploited to generate color changes in the presence of target analytes.

4.1.1. OXD-like activity-based sensing. The inherent OXD-like activity of Cu SAzymes, which catalyzes the oxidation of chromogenic substrates like TMB using O_2, serves as a direct signal generator. For instance, Ge and Yang's group designed a Cu-C-N SAzyme-based sensor with a reversible "on–off–on" response, enabling the sensitive detection of Hg^{2+} ions via cysteine-mediated inhibition (Fig. 7A).[75] Building on this principle, the same group developed a sensitive assay for α-glucosidase activity, where the enzyme's action on its substrate inhibited the OXD-like catalytic reaction (Fig. 7B), achieving a linear detection range of 0.25–8 U L^{-1} with an LOD of 0.09 U L^{-1}.[76] By leveraging the enhanced laccase-like catalytic activity of F-Cu nanozymes in the presence of thiram, Han et al. developed a straightforward and sensitive colorimetric method for thiram detection.[21] This intuitive and simple method facilitates the detection of thiram in the range of 0–7.5 μM and an LOD of 0.0845 μM.

4.1.2. POD-like activity-based sensing. The H_2O_2-dependent POD-like activity provides a versatile platform for detecting various antioxidants and biomolecules that can influence the H_2O_2-mediated oxidation process. For example, Cu SAzymes have been utilized for detecting antioxidants like ascorbic acid[77] and tannic acid (Fig. 7C),[69] as well as biomolecules like D-penicillamine (Fig. 7D),[78] based on their ability to scavenge intermediate ROS and suppress the colorimetric reaction. The high specificity of enzymatic reactions can be harnessed for sensing through specific inhibition. A notable example is the application of COF-derived Cu-NCNSs nanozyme for the real-time detection of amyloid-β (Aβ) monomer (Fig. 7E).[79] The coordination of Aβ monomers to the Cu active sites sterically hindered the POD-like activity, leading to a concentration-dependent decrease in color intensity and enabling real-time monitoring of amyloidogenesis with a linear range of 2.5–100 nM and an LOD of 1.18 nM. Furthermore, the sensing selectivity of Cu SAzymes can be precisely tuned at the atomic level by engineering their coordination environment. This principle is exemplified in the design of chiral Cu@L-His nanozymes, where the coordination of Cu with L-histidine creates a chiral microenvironment.[80] This structure enables enantioselective recognition and differential catalytic oxidation of D- and L-ascorbic acid, allowing for the distinct detection of total antioxidant capacity and the specific level of ascorbic acid.

4.1.3. Enzyme cascade systems. Coupling Cu SAzymes with natural enzymes creates powerful cascade systems for complex sensing tasks. Wu et al. constructed a cascade system involving acetylcholinesterase (AChE), choline oxidase (ChOx), and a Cu-N-C SAzyme for the dual detection of acetylcholine (ACh) and organophosphorus pesticides (OPs) (Fig. 7F).[81] ACh triggers the enzymatic cascade producing H_2O_2, while OPs inhibit AChE and further attenuate H_2O_2 production, achieving dual-purpose detection of ACh (linear range 10–8000 μM, LOD = 1.24 μM) and OPs pesticides (linear range 1–300 ng mL^{-1}, LOD = 0.60 ng mL^{-1}). Beyond the extra addition of natural enzymes, the nanozymes with multi-enzymatic activities facilitate the construction of a cascade system with robust stability and efficiency. Hamed et al. developed a Cu-SAN with both GAO- and
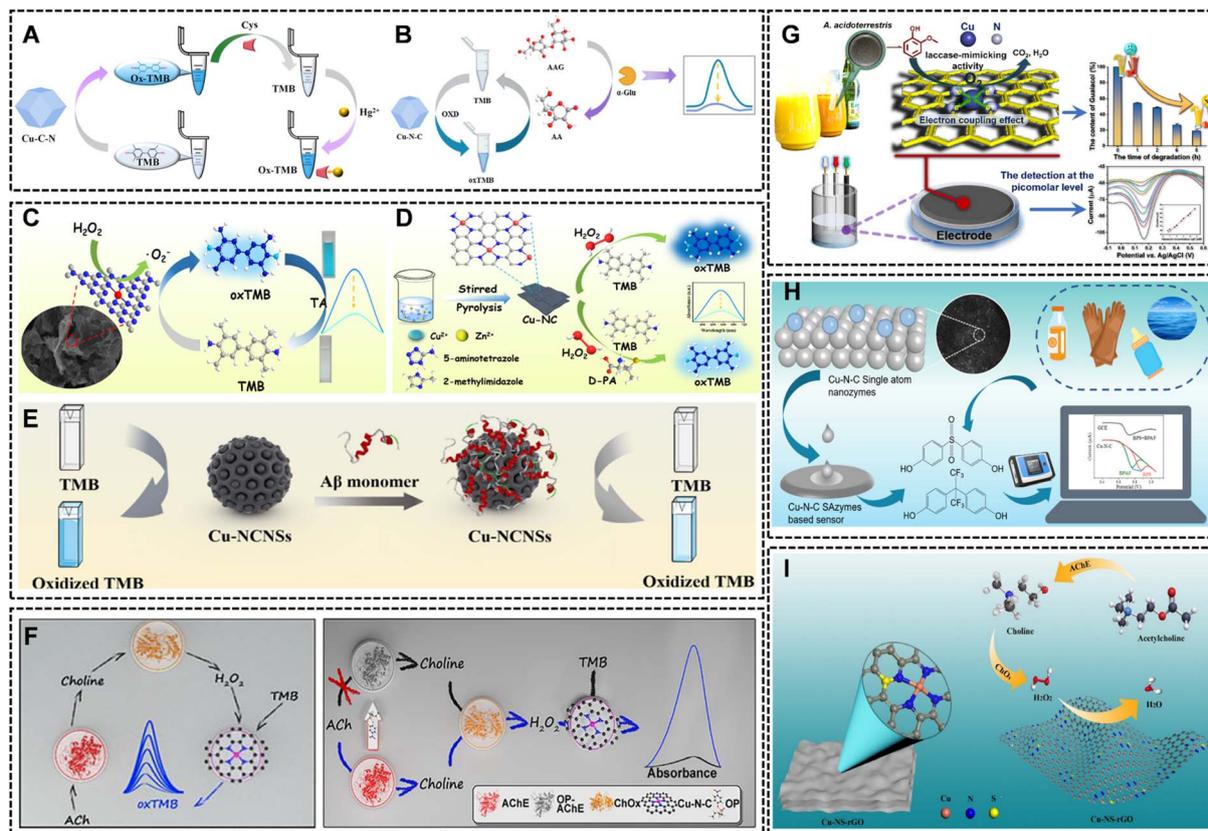
Fig. 7 (A) Illustration of the detection of Hg^{2+} ions based on SACu-C-N nanozyme with OXD-like activity. Reproduced with permission from ref. 75 Copyright (2024) Elsevier. (B) The sensing principle of the Cu-N-C SAzyme-based colorimetric sensor. Reproduced with permission from ref. 76 Copyright (2024) Elsevier. (C) Schematic diagram of TA colorimetric detection principle. Reproduced with permission from ref. 69 Copyright (2023) Elsevier. (D) Schematic diagram of D-PA colorimetric detection principle. Reproduced with permission from ref. 78 Copyright (2024) Elsevier. (E) Illustration of the Cu-NCNSs-based colorimetric sensing platform for Aβ monomer. Reproduced with permission from ref. 79 Copyright (2024) Springer-Verlag GmbH. (F) Schematic illustration of the ACC system for ACh and OP detection. Reproduced with permission from ref. 81 Copyright (2020) American Chemical Society. (G) Highly selective detection of guaiacol using CuN$_4$-G. Reproduced with permission from ref. 43 Copyright (2023) Elsevier. (H) Rapid detection of BPA, BPS, and BPAF *via* double-electron, double-proton electrochemical oxidation at Cu-Nx sites. Reproduced with permission from ref. 82 Copyright (2024) Elsevier. (I) Schematic of Cu-NS-rGO nanozyme application in choline (Ch) and acetylcholine (ACh) detection. Reproduced with permission from ref. 39 Copyright (2024) Elsevier.

POD-like catalytic activities for D-galactose detection.[45] Cu-SAN catalyzed the oxidation of D-galactose to produce H$_2$O$_2$ and subsequently decomposed to ˙OH for further TMB oxidation, facilitating the D-galactose detection with a linear range of 1–60 μM and an LOD of 0.23 μM.

Obviously, the strategies based on TMB or ABTS oxidation offer the supreme advantages of simplicity and low cost, making them ideal for point-of-care testing (POCT) and field deployable kits (*e.g.*, lateral flow assays). However, the sensitivity is often lower than electrochemical or fluorescence methods, and they can be susceptible to interference from colored samples or ambient light.

4.2 Electrochemical sensing

Electrochemical sensors benefit from the direct electron transfer capabilities and high catalytic efficiency of Cu SAzymes, offering rapid, sensitive, and quantitative analysis.

The laccase-like activity of CuN$_4$-G was exploited for the highly selective and sensitive detection of guaiacol, achieving a remarkably low LOD of 1.2 pM (Fig. 7G).[43] The stability and efficiency of nanozyme allowed for a wide logarithmic linear range, showcasing its potential for monitoring food spoilage. The superior catalytic capacity of Cu-N-C SAzymes has also been applied for the direct electro-oxidation of environmental pollutants, which enabled the simultaneous rapid detection of bisphenols (BPA, BPS, BPAF) *via* a two-electron, two-proton process at the isolated Cu-N$_x$ sites (Fig. 7H).[82] The well-resolved redox peaks and sensitive quantification of BPS in the 1–50 μM range (LOD = 50 nM), highlighting their potential for environmental monitoring. Furthermore, the high POD-like activity of Cu-NS-rGO was integrated into an enzymatic cascade for neurotransmitter detection.[39] In the presence of choline oxidase and acetylcholinesterase, the nanozyme electro-catalytically reduced the generated H$_2$O$_2$, enabling ultrasensitive detection of choline and acetylcholine with detection limits in the low nanomolar range (Fig. 7I).

The electrochemical methods possess extremely high sensitivity and a wide linear range, making them suitable for the detection of trace analytes in complex biological fluids.

However, the need for specialized electrode systems and portable potentiometers currently restricts their application outside centralized laboratories. The integration with microelectronic devices will be the key in the future.

4.3 Luminescence-based sensing

The integration of catalytic activity with luminescent signal readouts has opened avenues for highly sensitive and versatile sensing platforms.

For example, Liu *et al.* proposed a Cu-activated carbon dot@SiO$_2$ nanozyme combined POD-like activity with room-temperature phosphorescence (RTP).[83] The detection of glyphosate was based on its chelation with Cu^{2+} ions, which simultaneously inhibited the catalytic reaction (colorimetric mode) and restored the RTP emission (luminescent mode), providing complementary detection channels with high sensitivity (Fig. 8A). Similarly, the robust catalytic activity of Cu SAs@CN was leveraged to enhance the electrochemiluminescence (ECL) of the luminol-H$_2$O$_2$ system. Combining with a catalytic hairpin assembly (CHA) and CRISPR-Cas12a amplification strategy, this platform achieved an ultra-low detection limit of 1.09 fM for

miRNA-622 in serum, highlighting its potential for clinical diagnostics (Fig. 8B).[84]

4.4 Multimodal and smart sensors

Systems that combine color determination, photothermal, and electrochemical signals represent a powerful trend towards self-validating and highly reliable detection. It can effectively overcome the limitations of any single mode, enhance the credibility of the results, and increase the adaptability to different sample matrices. Cu SAzymes have been engineered into multimodal and stimulus-responsive systems for wide applications.

4.4.1. Dual-mode sensing platforms. The combination of two independent readout signals (*e.g.*, colorimetric and electrochemical, or colorimetric and fluorescent) has emerged to enhance reliability and provide built-in cross-validation. Liao *et al.* designed a Cu single-atom/atomic-cluster (Cu SAs/ACs@NC) nanozyme for the dual-mode detection of paracetamol (PA).[85] The single-atom sites enabled sensitive electrochemical detection of PA *via* its electro-oxidation, while the atomic clusters promoted the H$_2$O$_2$-TMB colorimetric reaction,
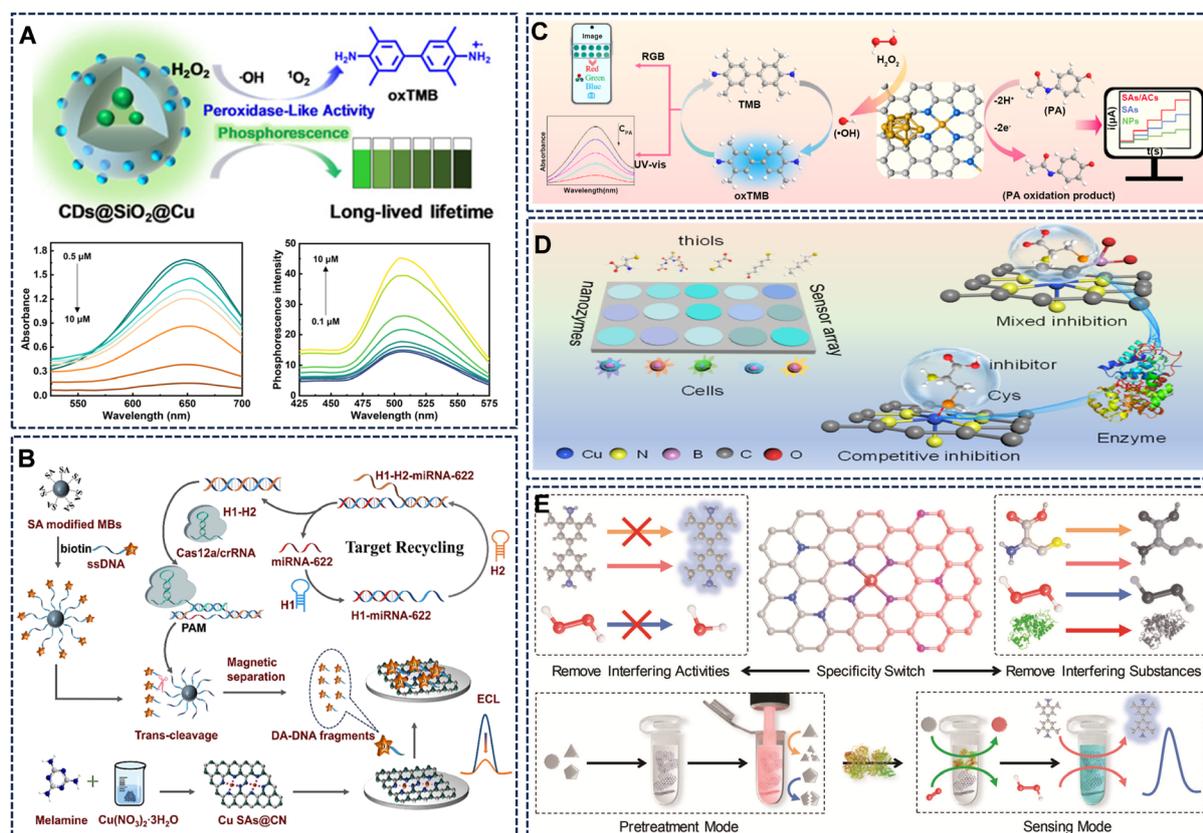
Fig. 8 (A) CDs@SiO$_2$@Cu that integrates neutral–pH POD-like activity and RTP. Reproduced with permission from ref. 83 Copyright (2025) The Royal Society of Chemistry. (B) Design principles of a novel ECL biosensor for miRNA-622 Detection. Reproduced with permission from ref. 84 Copyright (2024) American Chemical Society. (C) Schematic illustration of the electrochemical–colorimetric dual-mode detection mechanism of PA. Reproduced with permission from ref. 85 Copyright (2025) Elsevier. (D) Schematic diagram of pathological lesion recognition for various cell types and colorimetric response patterns of the sensor array for five cell types. Reproduced with permission from ref. 64 Copyright (2025) American Chemical Society. (E) Schematic diagram of light-thermal switchable Cu SA/NC for anti-interference detection. Reproduced with permission from ref. 47 Copyright (2023) Wiley-VCH.

which was quenched by PA (Fig. 8C). This provided two independent readouts for self-validating assays. Similarly, a Cu-TA nanosheet-based nanozyme was developed for the dual-mode (fluorescent and colorimetric) detection of quercetin, offering a self-verifying platform for complex sample analysis.

4.4.2. Sensor arrays for cell identification. Moving beyond single-analyte detection, a boron-doped Cu-N nanozyme (B₆/CuSA) was used to construct a colorimetric sensor array for thiol profiling.[64] The distinct interaction patterns between different thiols and the Cu-N and B-O sites generated unique absorbance response fingerprints, allowing for accurate discrimination of multiple thiols and classification of different cancer cell lines *via* chemometric analysis (Fig. 8D).

4.4.3. Stimulus-responsive smart sensing. To overcome interference in real samples, Zhu's group developed a photothermal-switchable Cu SA/NC nanozyme for interference-resistant sensing.[47] This "smart" system leveraged the temperature-dependent specificity of the nanozyme: at room temperature, it exhibited dominant POD-like activity for glucose detection, while under NIR irradiation, activated OXD- and CAT-like pathways cleared interferents (Fig. 8E). This allowed for accurate glucose quantification in untreated biological samples like serum and tumor lysates.

5. Antibacterial therapy

Nanozyme-based antibacterial strategies offer a potent alternative to conventional antibiotics, particularly in the fight against drug-resistant bacteria and stubborn biofilms. While the fundamental enzyme-like activities (*e.g.*, POD-like, OXD-like) of Cu SAzymes are common across different applications, their deployment in antibacterial therapy addresses distinct biological targets and challenges compared to those in cancer treatment. In this case, the primary goal is to directly destroy the structure of prokaryotic cells and combat resistant biofilms, which is completely different from the targets for eukaryotic
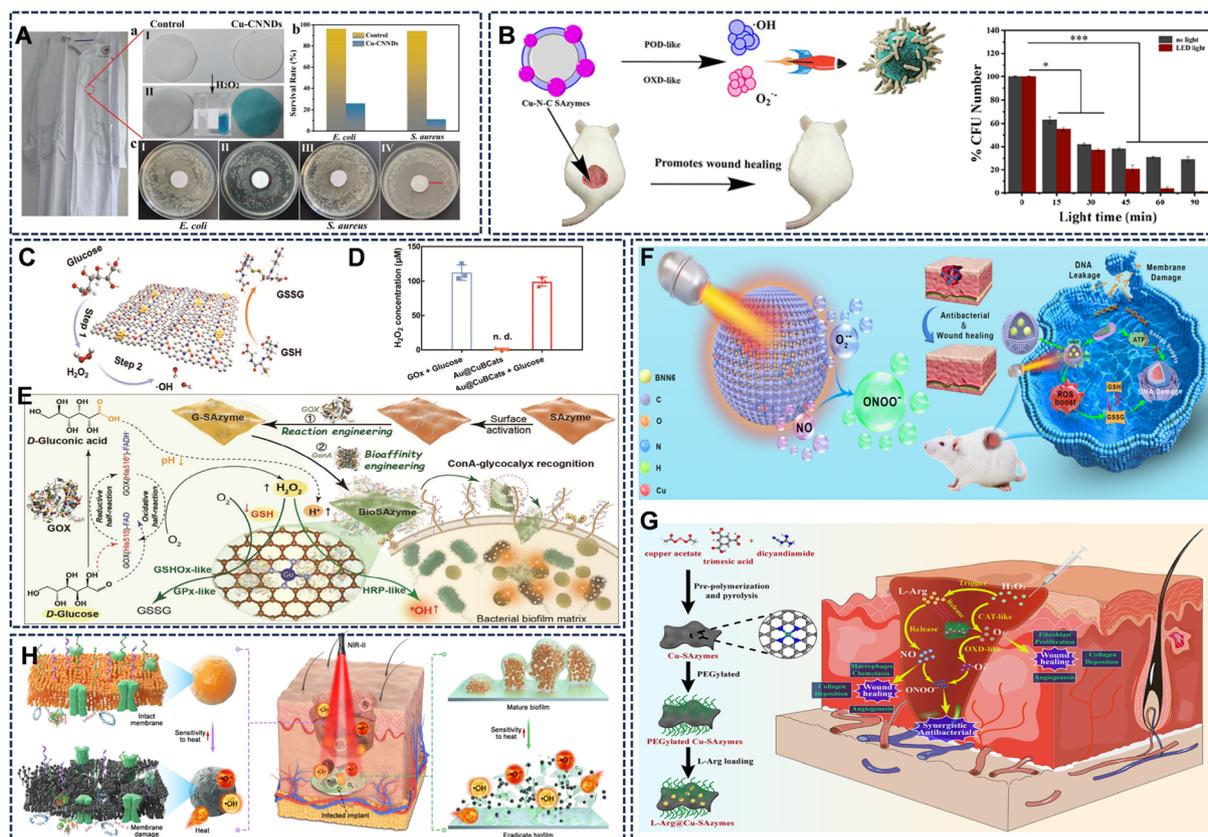
Fig. 9 (A) Atomic-layer-thin Cu-CNNDs exhibit outstanding broad-spectrum antibacterial properties under various conditions. Reproduced with permission from ref. 36 Copyright (2023) Wiley-VCH. (B) Cu-N-C can generate ˙OH and O₂˙⁻ in oxidase-catalyzed reactions, exhibiting excellent antibacterial effects that are further enhanced through photocatalytic action. Reproduced with permission from ref. 41 Copyright (2022) American Chemical Society. (C and D) Schematic illustration of Au@CuBCats as a dual-enzyme-mimetic platform for initiating cascade catalysis and GSH depletion, and the exceptional ability of Au@CuBCats to oxidize glucose into H₂O₂. Reproduced with permission from ref. 37 Copyright (2023) Wiley-VCH. (E) Schematic illustration of the synthesis and function of the BioSAzyme reactor. Reproduced with permission from ref. 46 Copyright (2024) Wiley-VCH. (F) Schematic illustration of the anti-infection application of Cu HSAz@BNN6. Reproduced with permission from ref. 68 Copyright (2025) Wiley-VCH. (G) Schematic illustration of the main mode of action for ʟ-Arg@Cu-SAzymes-based synergistic nanocatalytic therapy for MDR bacterial-infected wounds. Reproduced with permission from ref. 51 Copyright (2023) Elsevier. (H) antibacterial therapies from superficial to deep tissue infections. Reproduced with permission from ref. 42 Copyright (2023) Science and Technology Review Publishing House.

tumor cells. This section will therefore focus on Cu SAzyme designs and mechanisms specifically engineered to exploit bacterial vulnerabilities.

5.1 Direct catalytic bactericidal effects

The intrinsic enzyme-like activities of Cu SAzymes can be directly harnessed to generate a flux of ROS at the infection site. Notably, the bacterial cell membrane, rich in unsaturated lipids, is particularly susceptible to oxidative damage by radicals like ˙OH. The exceptional POD-like activity of atomically thin Cu-CNNDs was leveraged to create durable antibacterial coatings on cotton fabrics.[36] The ultrasmall size of the nanozymes facilitated close contact with microbes, enabling sustained intracellular ˙OH generation. This resulted in >99% bactericidal and fungicidal efficiency against *E. coli*, *S. aureus*, and *R. solani*, demonstrating potential for medical textiles (Fig. 9A). Cu-N-C nanozymes with combined intrinsic POD- and OXD-like activities were employed to simultaneously generate ˙OH and $O_2^{\cdot-}$, achieving efficient bacterial killing and biofilm disruption.[41] This catalytic activity was further enhanced under LED light, promoting rapid wound healing in murine infection models (Fig. 9B). The study on MN_4 (M = Cu, Co) structured SAzymes demonstrated that the CuN_4 configuration exhibits superior POD-, CAT-, SOD-, and NADPH oxidase (NOX)-like multi-enzymatic activities. When combined with low levels of H_2O_2, CuN_4 showed an impressive 82.2% antibacterial efficiency against *E. Coli* by significantly enhancing intracellular ROS accumulation.[86] Furthermore, the design of carbon dot-based Cu nanozymes (Cu-CDs) with POD-like and OXD-like activities has been reported to effectively kill bacteria through ROS generation, while their inherent antioxidant (SOD-like) activity can also help modulate oxidative stress in the wound microenvironment, presenting a dual-function strategy for infected wound therapy.[87]

Thus, the direct catalytic killing strategy is most suitable for surface prevention and prophylaxis, such as on biomedical implants, textiles, or wound dressings. However, its efficacy may be limited against established, dense biofilms or in deep-seated infections due to poor penetration and potential depletion of local substrate (*e.g.*, H_2O_2).

5.2. Cascade catalysis for enhanced efficacy

Cascade reactions, which mimic metabolic pathways in cells, can significantly amplify antibacterial efficacy by producing high local concentrations of ROS and depleting protective antioxidants. For example, Fan *et al.* developed a dual-enzyme-mimetic bionanocatalyst (Au@CuBCats) integrating GOx-mimetic Au nanoparticles with POD-mimetic Cu-N_2O_1 single-atom sites (Fig. 9C).[37] This system initiated a two-step cascade: glucose oxidation to generate H_2O_2, followed by its conversion into highly toxic ˙OH (Fig. 9D). This simultaneous nutrient depletion and ROS storm effectively overwhelmed bacterial defenses, showing great efficacy against multidrug-resistant bacteria in diabetic ulcer models. To address the challenge of biofilms, Huang *et al.* designed a protein-directed single-atom bionanozyme (BioSAzyme) combining a Cu

SAzyme with natural GOx and the targeting molecule concanavalin A (ConA) (Fig. 9E).[46] ConA provided specific binding to the biofilm glycocalyx. The GOx then generated a localized, acidic environment rich in H_2O_2, which was utilized by the multi-enzyme active Cu-N_4 sites to produce ˙OH and deplete the GSH in the biofilm. This multi-pronged attack effectively disrupted the extracellular polymeric matrix and eradicated biofilms of pathogenic *E. coli* and MRSA.

This approach performs particularly well in environments where there are high levels of endogenous substrates, such as diabetic wounds with high concentrations of glucose. By self-supplying H_2O_2 and converting it to toxic ˙OH, it creates a powerful, localized oxidative burst. However, the treating efficiency relies on a specific supply of substrates, which may vary depending on the location of the infection.

5.3. Stimulus-responsive and synergistic systems

Spatiotemporal control over catalytic activity, achieved through external stimuli like light, allows for on-demand, localized treatment with enhanced precision and reduced off-target effects.

For example, A hollow Cu SAzyme (Cu HSAz) responsive to NIR-II light was designed to co-deliver a nitric oxide (NO) donor (BNN6) (Fig. 9F).[68] Upon irradiation, the photothermal effect triggered NO release, which reacted with the $O_2^{\cdot-}$ (generated by the OXD-like activity) to form a high density of peroxynitrite (ONOO⁻). This powerful oxidant disrupted bacterial membranes, depleted energy and antioxidants, and caused DNA fragmentation, leading to the complete eradication of MRSA-infected wounds. Qiu *et al.* engineered an L-arginine-loaded Cu SAzyme (L-Arg@Cu-SAzyme) to execute a sophisticated ROS/RNS cascade (Fig. 9G).[51] The CAT- and OXD-like activity of Cu SAzyme first generated O_2 and $O_2^{\cdot-}$, while the tumor microenvironment triggered NO release from L-arginine. The subsequent coupling of NO and $O_2^{\cdot-}$ produced ONOO⁻, creating a powerful oxidative/nitrosative stress that dismantled biofilms and accelerated the healing of MRSA-infected wounds, promoting anti-inflammatory responses, angiogenesis, and collagen deposition. Wu *et al.* further stimulated the GOx-like activity as well as the POD-like activity with light irradiation, which is responsible for ROS generation by a cascade reaction to eradicate Gram-positive and Gram-negative multidrug-resistant bacteria.[88]

These stimulus-responsive and synergistic therapeutic approaches represent the most advanced paradigm for precision treatment of complex and deep-seated infections. The spatiotemporal control minimizes off-target damage to healthy tissue. The integration of multiple killing mechanisms (ROS, RNS, cuproptosis, photothermal) addresses heterogeneity and resistance. However, the complexity of design and the need for external stimulus restrict the wide-scale application.

5.4. Integration of physical and chemical modalities

Combining the catalytic activity of Cu SAzymes with physical energy conversion, such as photothermal effects, creates a powerful synergistic approach to overcome multidrug

resistance. Bai *et al.* designed an ultrathin 2D CuN$_4$-CNS nanozyme to combine triple enzyme-mimetic activities (POD, CAT, OXD) with high NIR-II photothermal conversion efficiency (Fig. 9H).[42] The system continuously generated ˙OH and O$_2$˙$^-$, while the localized photothermal heating (~48 °C) accelerated ROS production and disrupted membrane integrity. This synergy enabled the eradication of both planktonic bacteria and entrenched biofilms on implants, effectively treating both superficial and deep-tissue infections. Similarly, Cu SASs/NPC nanozymes with Cu-N$_4$ centers and an exceptional 82.8% photothermal conversion efficiency achieved >99% killing of *E. coli* and *MRSA in vitro* under 808 nm irradiation, and significantly accelerated wound healing *in vivo* through the combined action of ROS, GSH depletion, and hyperthermia.[71]

Overall, the choice of strategy should be guided by the infection profile. The direct catalytic coating strategies are ideal for surface protection, and cascade catalysis systems can provide self-enhanced killing effects for substrate-rich local infections. For deep, persistent, or biofilm-associated infections that require precise, potent, and multi-mechanistic intervention, stimulus-responsive synergistic systems are the most promising approach. Future designs should increasingly focus on environmentally adaptive nanozymes that can dynamically switch or combine these modalities according to the infection microenvironment (such as pH, enzyme, or glutathione levels).

6. Anticancer therapy

In contrast to the direct killing objectives in antibacterial therapy, Cu SAzymes-based anticancer strategies must navigate the complex and immunosuppressive TME. The therapeutic focus shifts to regulating specific programmed cell death pathways in eukaryotic cells and reshaping the tumor microenvironment to achieve sustained immune monitoring.[89] This section delineates the major strategic paradigms in which Cu SAzymes are employed to achieve enhanced antitumor efficacy.

6.1 Synergistic catalytic cascade and cell death pathways

Moving beyond simple ROS generation, Cu SAzymes can be designed to orchestrate complex intracellular cascades that activate specific programmed cell death pathways, such as cuproptosis and ferroptosis, for a more potent and mechanistically diverse attack.[90] Specifically, cuproptosis is a novel form of regulated cell death driven by intracellular copper accumulation, leading to toxic aggregation of lipoylated proteins in the mitochondria.[91] Cu SAzymes can release Cu^{2+} ions in the reducing TME, which directly disrupt mitochondrial metabolism and induce cuproptosis.

For instance, Liu *et al.* developed a defective-copper-based MOF single-site nanozyme (F@D-CHTP SN) that exposed highly active sites that simultaneously generate intense ROS and release Cu^{2+} ions upon degradation (Fig. 10A).[57] This dual action effectively triggered a combination of cuproptosis and ferroptosis. Furthermore, the co-delivery of a STING agonist and a VEGFR inhibitor *via* this platform remodeled the tumor vasculature and immunosuppressive TME, leading to enhanced

T-cell infiltration and potent antitumor immunity. Similarly, Zhang *et al.* designed a Cu SAzyme embedded in disulfide-bridged dendritic mesoporous organosilica (CDPh), which can release the atomically dispersed Cu-O$_2$/Cu-O$_4$ sites under high-GSH conditions of the TME (Fig. 10B).[58] This initiated ROS production and GSH depletion. The synergistic effect was amplified by the co-delivered phloretin, which inhibited glucose uptake. This metabolic interference collaborated with the catalytic activity to induce DLAT-dependent cuproptosis, achieving nearly complete tumor suppression with minimal side effects. In another work, Cu(I)-anchored C$_3$N$_4$ nanofibers (Cu-CN) served as a bifunctional catalyst, mimicking both glutathione oxidase and peroxidase activities (Fig. 10C).[70] This enabled a self-cascade process: oxidizing GSH to produce H$_2$O$_2$, which was subsequently converted into highly toxic ˙OH. The resulting collapse of the redox balance induced extensive lipid peroxidation, effectively activating ferroptosis/apoptosis pathways and achieving strong tumor growth inhibition.

This synergistic catalytic cascade strategy relies solely on excessive H$_2$O$_2$ and an acidic environment, which exhibits advantages in its tumor selectivity and low requirement for external intervention. However, the therapeutic effectiveness is often limited by the insufficient and heterogeneous endogenous H$_2$O$_2$ in many solid tumors, resulting in incomplete therapy.

6.2 External energy-based synergistic therapy

The integration of external energy sources, such as light and radiation, with Cu SAzymes enables spatiotemporal control over therapy, enhancing tumor ablation while overcoming common therapeutic barriers like hypoxia.

6.2.1. Photothermal/chemodynamic synergy. Single-atom Cu-MXene nanozymes were incorporated into bone scaffolds for the treatment of osteosarcoma (Fig. 10D).[65] The Cu sites provided POD- and GSHOx-like activities for chemodynamic therapy (CDT), while the material itself served as an efficient photothermal agent. Upon NIR irradiation, the mild hyperthermia generated not only directly damaged tumor cells but also accelerated the ROS production and lipid peroxidation, synergizing with the catalytic activity to enhance ferroptosis (Fig. 10E), achieving a synergistic antitumor and tissue-reconstructive effect.

6.2.2. NIR-enhanced tumor penetration. Inspired by jellyfish, Xing *et al.* developed Cu single-atom nanomotors (Cu-JMCNs) to overcome poor tumor penetration.[92] The Cu centers catalyzed H$_2$O$_2$ for CDT and oxidized GSH. Upon 980 nm irradiation, the nanomotors exhibited self-thermophoretic motion, driven by anisotropic thermal gradients, which significantly enhanced their diffusion and penetration deep into tumor tissues. This active delivery strategy markedly improved the therapeutic efficacy of the combined CDT and PTT (Fig. 10F).

6.2.3. Radiotherapy sensitization. Cu SAzymes can potently sensitize tumors to radiotherapy (RT) by simultaneously alleviating hypoxia and amplifying oxidative damage. Wu *et al.* designed a CuN$_3$-centered SAzyme with robust POD-like activity, which converted H$_2$O$_2$ into highly toxic ˙OH radicals, leading to
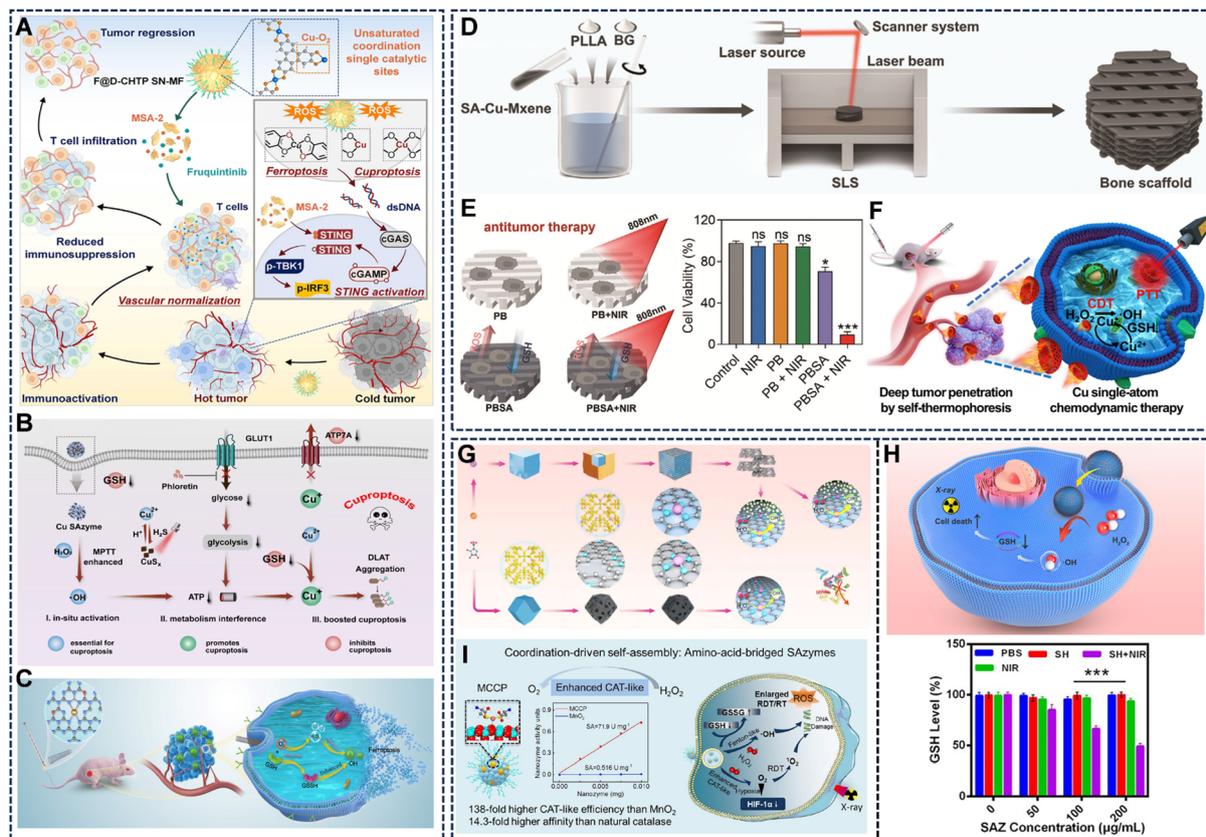
Fig. 10 (A) Schematic illustration of tumor therapy mechanism mediated by F@D-CHTP SN-MF. Reproduced with permission from ref. 57 Copyright (2024) Elsevier. (B) Schematic illustration of the antitumor performance of CDPh in CT26 tumor cells. Reproduced with permission from ref. 58 Copyright (2024) Wiley-VCH. (C) The Cu-CN, as a bifunctional enzyme, mimics tumor cascade catalytic therapy. Reproduced with permission from ref. 70 Copyright (2023) Elsevier. (D) Synthetic procedure of PLLA/BG/SA-Cu-MXene composite bone scaffolds. Reproduced with permission from ref. 65 Copyright (2024) Wiley-VCH. (E) Under NIR irradiation, this system generates mild hyperthermia to enhance antitumor efficacy. Reproduced with permission from ref. 65 Copyright (2024) Wiley-VCH. (F) NIR light-driven active movement for enhanced penetration of *in vivo* tumors by self-thermophoretic diffusion, and subsequent CDT and PTT combined therapy. Reproduced with permission from ref. 92 Copyright (2023) American Chemical Society. (G) Schematic diagram of the synthesis strategy of CuN$_3$-SAzyme and CuN$_4$-SAzyme. Reproduced with permission from ref. 55 Copyright (2024) Springer Nature. (H) NIR-triggered release promotes ˙OH generation and efficiently reduces intracellular GSH levels. Reproduced with permission from ref. 40 Copyright (2024) IOP Publishing Ltd. (I) Schematic illustration of the structure and electron transfer process of MCCP with enhanced CAT-like activity for increasing O$_2$ generation. Reproduced with permission from ref. 66 Copyright (2023) American Chemical Society.

DNA breaks and apoptosis.[55] By integrating NIR irradiation and X-ray exposure, this system created a dual-field ROS storm that effectively relieved hypoxia and led to complete tumor eradication (Fig. 10G). In another approach, a light-responsive hydrogel encapsulating Cu SAzymes was developed for on-demand therapy.[40] NIR-triggered release facilitated simultaneous ˙OH generation and GSH depletion, which profoundly sensitized tumors to low-dose radiotherapy, resulting in significant tumor regression (Fig. 10H). Furthermore, PVP-modified MoO$_x$-Cu-Cys SAzymes (MCCP) were designed to exhibit CAT-like activity for O$_2$ generation and Fenton-like activity for ˙OH/^{1}O$_2$ production.[66] Under X-ray irradiation, this ROS cascade, coupled with GSH oxidation, created a highly cytotoxic environment that dramatically enhanced the outcomes of radiotherapy (Fig. 10I).

Introducing external triggers (such as NIR, ultrasound, and self-powered electric field) enables spatial and temporal control as well as on-demand activation, thereby significantly

enhancing the catalytic activity beyond the natural limits within the body. This strategy is highly effective but requires tumor accessibility to the stimulus and adds complexity to treatment protocols.

6.3 Synergy with immunotherapy

Cu SAzymes can act as immunomodulatory agents by inducing immunogenic cell death (ICD) and reversing the immunosuppressive TME, thereby bridging localized tumor destruction with systemic antitumor immunity.

**6.3.1. Photothermal-enhanced immunogenic cell death.** Ye *et al.* developed a Cu-N$_4$ SAzyme that integrated POD-like catalysis with photothermal conversion to trigger robust ICD.[93] Under 808 nm NIR irradiation, the combined ˙OH generation and hyperthermia promoted the exposure of damage-associated molecular patterns (*e.g.*, calreticulin, HMGB1), which in turn stimulated dendritic cell maturation

and activated CD8$^+$ T-cells, establishing a potent and sustained antitumor immune response (Fig. 11A).

6.3.2. Bioorthogonal catalysis and cuproptosis. Wu *et al.* further designed a bioorthogonal Cu single-atom catalyst (CuSACO) to selectively anchor onto tumor cells *via* click chemistry.[48] Its multi-enzyme activities (CAT, OXD, POD) generated a ROS burst, while the GSH-mediated release of Cu ions initiated cuproptosis (Fig. 11B). The combination of these effects, augmented by photothermal therapy, triggered potent ICD, boosted T-cell infiltration, and effectively reversed the immunosuppressive TME. Furthermore, Chen *et al.* designed a Cu SAzyme-based radioimmunotherapy for breast cancer (Fig. 11C).[94] Under acidic TME, Cu SAzyme catalyzed H_2O_2 into ˙OH and oxidized GSH, enhancing ROS-mediated DNA double-strand breaks under radiotherapy. The induced ICD enhanced CD8$^+$ T-cell infiltration and elevated pro-inflammatory cytokines, highlighting the powerful synergy between oxidative stress and immune activation.

6.3.3. Metabolic interference-triggered pyroptosis. Niu *et al.* reported a sulfur-doped Cu SAzyme (Cu-NS@UK@POx) that combined cascade biocatalysis with programmed pyruvate metabolism therapy (Fig. 11D).[19] By depleting key metabolites and generating an ˙OH storm, it induced caspase-1/GSDMD-dependent pyroptosis, while inhibition of pyruvate import and oxidation reoxygenated the TME, promoted M1 macrophage polarization, and enhanced T-cell recruitment, producing robust systemic antitumor responses (Fig. 11E). Expanding toward metabolic regulation, Xu *et al.* constructed a Cu SA-DOX@COD platform for prostate cancer immunotherapy (Fig. 11F).[49] The multi-enzyme-like activities of Cu SAzyme depleted GSH and enhanced tumor oxygenation, while co-loaded cholesterol oxidase (COD) disrupted cholesterol metabolism. This metabolic interference, combined with doxorubicin-induced caspase-3/GSDME cleavage, effectively triggered pyroptosis and activated a comprehensive antitumor immune response.
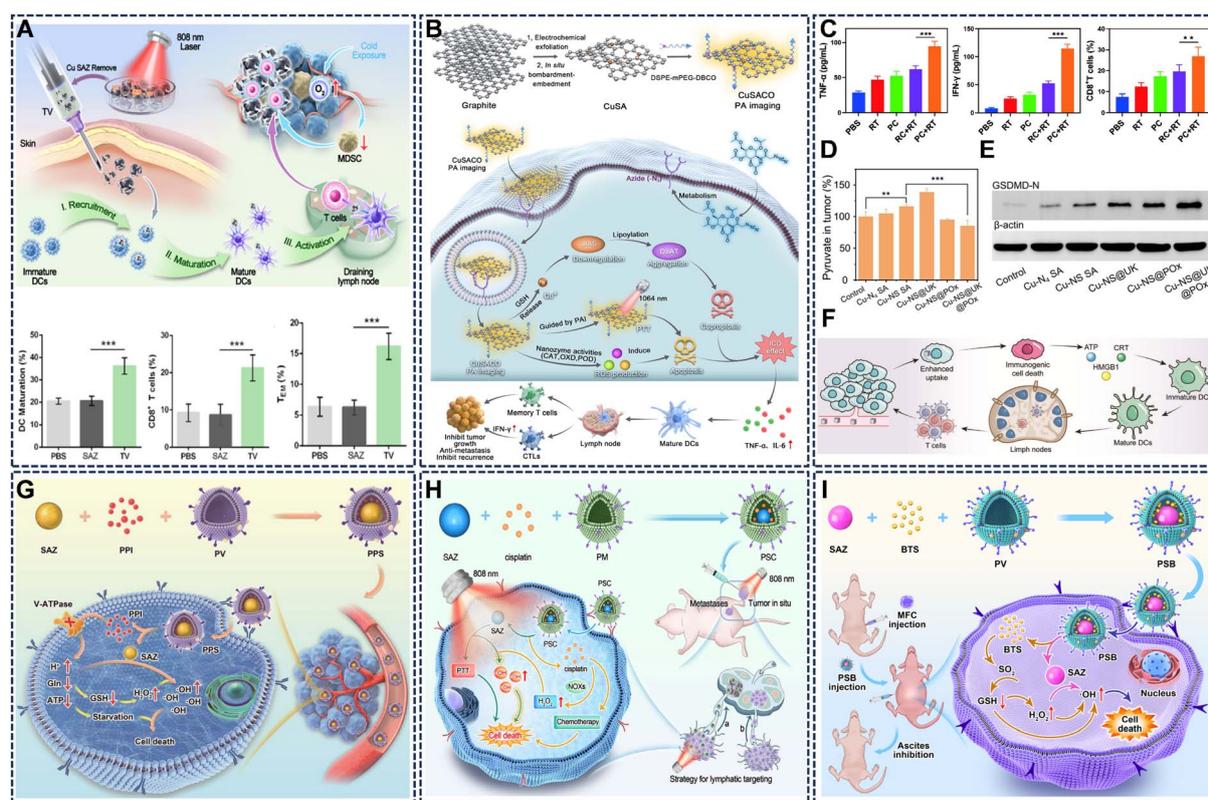
Fig. 11 (A) The ability to best promote dendritic cell maturation and sustained immune competence. Reproduced with permission from ref. 93 Copyright (2025) American Chemical Society. (B) CuSACO efficiently targets tumors through a bioorthogonal click reaction with azide groups on cell surfaces *via* a membrane turnover mechanism. Reproduced with permission from ref. 48 Copyright (2024) Wiley-VCH. (C) Characteristics of tumor-infiltrating lymphocytes were analyzed across treatment groups to evaluate the feasibility of PC-enhanced radiotherapy for activating immunotherapy. Reproduced with permission from ref. 94 Copyright (2024) Dove Medical Press Ltd. (D) Pyruvate levels in tumor tissue cells were significantly downregulated in the Cu-NS@UK@POx group. Reproduced with permission from ref. 19. Copyright (2024) Wiley-VCH. (E) Cu-NS SA, with its stronger enzyme activities, can more effectively trigger pyroptosis than Cu-N$_4$ SA. Reproduced with permission from ref. 19 Copyright (2024) Wiley-VCH. (F) Schematic diagram of the construction and antitumor immunotherapy mechanism of Cu SA-DOX@COD. Reproduced with permission from ref. 49 Copyright (2024) Wiley-VCH. (G) Schematic illustration of a biomimetic SAzyme system for self-enhanced NCT. Reproduced with permission from ref. 95 Copyright (2022) Springer Nature. (H) Schematic illustration of biomimetic SAzyme synergistic chemotherapy against gastric cancer lymphatic metastasis. Reproduced with permission from ref. 96 Copyright (2025) Wiley-VCH. (I) Schematic diagram showing the biomimetic SAzyme system for efficient inhibition of gastric cancer ascites *via* SO$_2$ gas-enhanced nanocatalytic cancer therapy. Reproduced with permission from ref. 97 Copyright (2023) Elsevier.

6.4 Targeted delivery systems

Precise delivery to tumor tissues is crucial for maximizing therapeutic efficacy and minimizing systemic toxicity. Biomimetic strategies have been widely adopted to improve the targeting capability of Cu SAzymes.

6.4.1. Biomimetic platelet membrane coating. A platelet-membrane-cloaked Cu SAzyme (PPS) was developed for the treatment of gastric cancer and its lymphatic metastasis.[95,96] The platelet membrane conferred active targeting to CD44-overexpressing tumor cells *via* P-selectin interactions, prolonging circulation and enhancing tumor accumulation. The catalytic Cu-N_4 centers generated $\cdot$OH, while co-delivered drugs (*e.g.*, pantoprazole or cisplatin) acidified the TME, blocked GSH synthesis (Fig. 11G), or caused DNA damage (Fig. 11H). This created a self-amplifying therapeutic cycle, leading to potent tumor suppression and apoptosis. This platform was further advanced by co-loading an SO_2 prodrug, where the released SO_2 reacted with $\cdot$OH to generate more reactive $\cdot SO_3^-$ radicals, deplete GSH, and elevate H_2O_2 levels, resulting in a highly efficient gas-enhanced nanocatalytic therapy (Fig. 11J).[97] Furthermore, Guo *et al.* developed a Cu SAzyme camouflaged with a 4T1 tumor cell membrane (M@Cu SAC).[98] This platform not only enhances tumor accumulation through homologous targeting but also combines CDT with mild PTT. The membrane coating improves biocompatibility and the platform's ability to catalyze $\cdot$OH generation in the TME, while enabling real-time tumor monitoring *via* photoacoustic imaging, representing an advanced theranostic approach for precise cancer treatment.

6.4.2. Protein-supported pathogen-targeting. Beyond platelet-cloaking systems, Wang *et al.* introduced a bovine serum albumin-supported Cu SAzyme (BSA-Cu SAN) for colorectal cancer treatment.[38] The Cu-N_2O_2 sites enabled efficient $\cdot$OH generation and GSH depletion. Notably, this system also demonstrated potent activity against *Fusobacterium nucleatum*, a bacterium known to promote tumor growth and therapy resistance. By simultaneously eradicating the pathogen and exerting catalytic antitumor effects, it successfully disrupted the pathogen-tumor symbiosis, leading to significantly improved therapeutic outcomes.

Overall, these approaches exhibit great potential in anti-cancer therapy. The selection of suitable strategies should be matched with the tumor profiling. For superficial or manageable tumors with moderate oxidative stress, external stimulation often yields significant results. However, for deep, heterogeneous, and resistant tumors, a combined approach is indispensable. Future development lies in the "closed-loop" intelligent system, in which Cu SAzyme not only performs treatment but also senses specific TME biomarkers (such as pH, GSH, and adenosine triphosphate), and autonomously switches or combines its catalytic mode as needed, thereby achieving truly personalized and dynamic treatment.

7. Anti-inflammatory therapy

Inflammation is often driven by a cascade of reactive oxygen and nitrogen species (RONS). Cu SAzymes, functioning as robust catalytic scavengers, can intervene at various stages of this process. Their therapeutic strategies progress from the targeted elimination of specific RONS to the sequential disruption of the entire oxidative stress cascade, offering solutions for a spectrum of inflammatory conditions.

The $O_2^{\cdot-}$ is a primary ROS that initiates inflammatory signaling and can damage cellular components. The strategic design of Cu SAzymes as highly specific SOD mimics allows for the interception of inflammation at its earliest stage. For instance, Lu *et al.* engineered Cu/graphene oxide SAzymes (Cu/GO SACs) for exceptional specificity, mimicking SOD activity without engaging in pro-oxidant side reactions (Fig. 12A).[53] This precise targeting enabled the safe and effective removal of $O_2^{\cdot-}$, as demonstrated in models of cigarette smoke-induced oxidative stress, positioning them as a viable option for preventing airway inflammation. For treating severe systemic inflammation like sepsis, Cu-N_4 SAzymes were developed as highly stable and efficient SOD mimics (Fig. 12B).[52] In a murine sepsis model, these nanozymes effectively neutralized $O_2^{\cdot-}$, leading to a significant reduction in systemic pro-inflammatory cytokine levels (TNF-α and IL-6), alleviation of multi-organ injury, and a marked improvement in survival rates. For these single-enzyme mimic systems, the therapy efficiencies are usually straightforward and modular. However, inflammatory cascades often involve multiple, interdependent RONS; neutralizing one may not be sufficient to halt the entire oxidative stress cascade.

In chronic inflammatory diseases, multiple RONS are present and interconnected. Advanced Cu SAzymes can be designed to perform multi-step catalytic cascades, mimicking the body's natural antioxidant enzyme systems for more comprehensive protection. A sophisticated nanozyme (Cu-N_4ClG) was constructed to execute sequential SOD- and CAT-like activities (Fig. 12C).[63] This design enabled the continuous elimination of $O_2^{\cdot-}$ and the subsequent decomposition of the resulting H_2O_2 into harmless O_2. In osteoarthritis models, this multi-level ROS scavenging significantly decreased oxidative stress in chondrocytes, reduced cell apoptosis, and slowed cartilage degradation. The activity could be further enhanced by near-infrared photothermal stimulation, offering a synergistic strategy for managing chronic joint diseases. Systems mimicking SOD/CAT-like activities sequentially dismantle the ROS network. This broad-spectrum, "firewall" approach is more robust for chronic or complex inflammatory diseases where multiple RONS coexist and perpetuate inflammation. Their superior efficacy comes at the cost of a more intricate design.

The most complex strategies are no longer merely about eliminating reactive oxygen species. Instead, they can actively re-adjust the inflammatory microenvironment and promote tissue repair. This is an ideal strategy for inflammatory diseases accompanied by tissue damage. Cu SAzymes can be tailored to function inside cells, bolstering the endogenous antioxidant defense system. Chen *et al.* further developed Cu single atoms supported on graphitic carbon nitride (Cu SAs/CN) with intensive APX-like activity (Fig. 12D).[56] By utilizing intracellular ascorbate to reduce H_2O_2 to water, these nanozymes effectively shielded cells from H_2O_2-induced oxidative stress and apoptosis
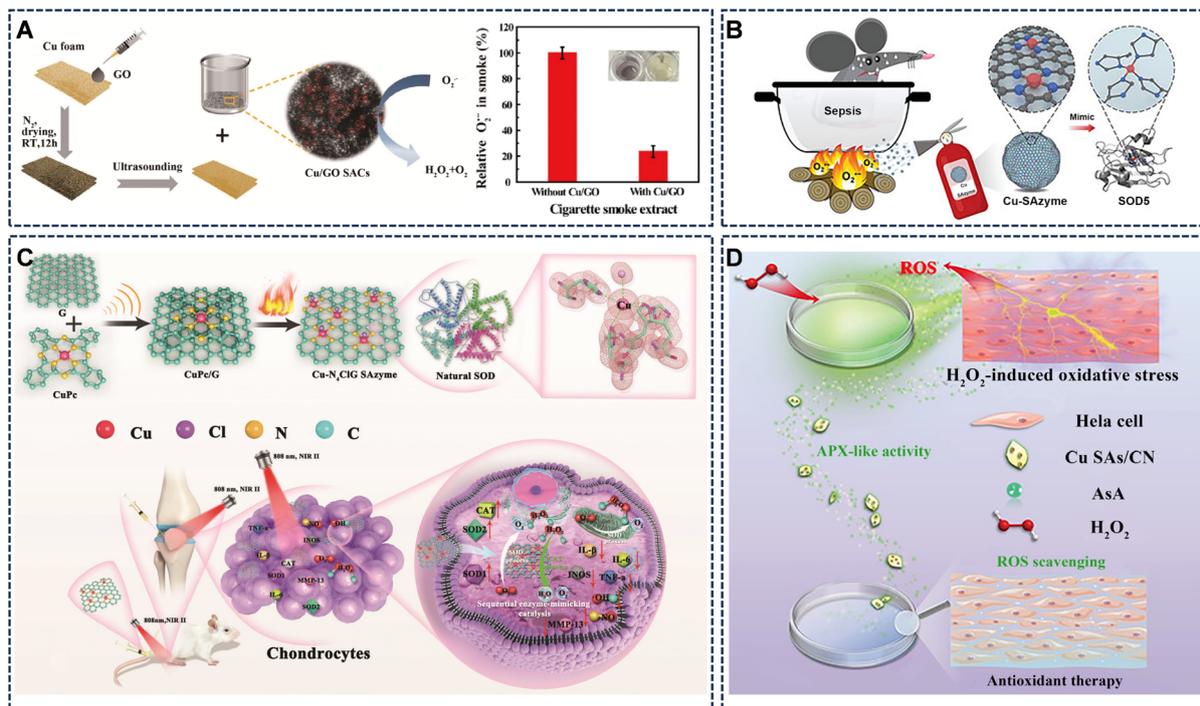
Fig. 12 (A) Schematic diagram of the synthesis of Cu/GO SACs and the SOD-mimetic process, along with their high efficiency in scavenging $O_2^{\bullet-}$. Reproduced with permission from ref. 53 Copyright (2022) Springer Nature. (B) This nanozyme efficiently scavenges $O_2^{\bullet-}$, inhibits TNF-α and IL-6 secretion, and effectively reduces mortality. Reproduced with permission from ref. 52 Copyright (2022) John Wiley and Sons. (C) Chematic illustrations on Cu-N4ClG SAzyme synthesis and the principles of biomimetic SOD and CAT for ROS scavenging. Reproduced with permission from ref. 63 Copyright (2022) Wiley-VCH. (D) Cu SAs/CN, owing to their inherent high-efficiency nanozyme activity mimicking APX and excellent biocompatibility, have been employed to effectively shield cells treated with H_2O_2 in vitro from oxidative damage. Reproduced with permission from ref. 56 Copyright (2021) Wiley-VCH.

in vitro, highlighting their potential for mitigating inflammation at the cellular level and preventing oxidative damage.

8. Summary and perspectives

Cu SAzymes have emerged as a transformative platform in artificial enzyme technology, characterized by their atomically dispersed copper active sites that enable high catalytic efficiency, tunable activities, and multi-enzyme mimicry. Through rational design of the local coordination environment, Cu SAzymes can simulate diverse natural enzymes, including POD, OXD, CAT, and SOD. As comprehensively discussed in this review, these properties have facilitated broad biomedical applications, ranging from sensitive biosensing and antibacterial therapy to anticancer treatments and anti-inflammatory interventions via ROS scavenging. By bridging atomic-level precision with biomedical functionality, Cu SAzymes exemplify the potential of nanozyme technology to advance precision medicine.

Despite the promising progress, current research on Cu SAzymes remains largely fragmented between fundamental material discovery and proof-of-concept biological demonstrations. A critical gap exists between their impressive in vitro performance and the stringent requirements for clinical translation. Three major challenges must be urgently addressed:

(1) Long-term biosafety and pharmacological uncertainties: the clinical application of Cu SAzymes is severely hindered by an incomplete understanding of their in vivo behavior. While cuproptosis is a leveraged mechanism for therapy, uncontrolled Cu(I)/(II) release poses a significant risk of off-target toxicity to copper-sensitive organs. The pharmacological profile of Cu SAzymes starkly contrasts with that of FDA-approved copper-based agents, which are used under strict, protocol-defined pharmacokinetic control. Comprehensive toxicology studies establishing maximum tolerated doses are scarce. Furthermore, interactions with the immune system and dominant clearance routes are poorly characterized, directly impacting bioavailability, therapeutic window, and potential for chronic inflammation. The metabolic fate of these inorganic-organic hybrids is largely unknown, raising unanswered questions about potential accumulation, degradation products, and long-term tissue responses.

(2) Manufacturing and characterization reproducibility: the catalytic performance of Cu SAzymes is extremely sensitive to the atomic coordination structure. Minor changes in synthesis parameters can lead to differences in active sites between batches, thereby making the catalytic activity unpredictable and non-reproducible. The lack of standardized protocols for synthesis, purification, and activity benchmarking hinders comparative analysis and reliable scale-up.

(3) Activity regulation and selectivity in complex biological environments: while multi-enzyme activity is an advantage, it is still challenging to temporally and spatially control specific activities in dynamic and mutually interfering TME or infection sites. Overcoming substrate competition, achieving tumor-selective activation over healthy tissues, and ensuring sufficient catalytic efficiency under physiological conditions are all difficult problems.

Looking ahead, subsequent research must shift from a purely activity-based approach to a comprehensive, translation-oriented model. To bridge the gap between the laboratory and clinical settings, a series of collaborative efforts should be conducted:

(1) Safety design and clearable architectures: priority should be given to engineering biodegradable or readily clearable Cu SAzymes. The strategies that can be adopted include designing ultra-small sizes (<6 nm) for efficient renal clearance, incorporating responsive linkers that trigger disintegration into non-toxic components after treatment, or using endogenous biomolecules for *in situ* synthesis and subsequent metabolic clearance. At the same time, strict long-term toxicology studies in accordance with Good Laboratory Practice (GLP) standards must be conducted.

(2) Standardization and scalable manufacturing: this field requires the establishment of standardized protocols for the synthesis of Cu SAzymes, physicochemical characterization (especially atomic coordination verification), and enzymatic kinetic assay. The development of robust, scalable, and green synthetic methods is crucial for repeatable large-scale production.

(3) Precision and intelligent catalysis: the next generation of designs must integrate multiple targeting and activation strategies to maximize therapeutic specificity and minimize side effects. This includes conjugating active targeting ligands for cell recognition and designing "switches" (pH values, redox, enzymes) that respond to the disease microenvironment. The goal is to strictly limit catalytic activity to the pathological site, thereby constructing a "closed-loop" therapeutic system that can autonomously respond to biomarkers.

(4) Synergistic platforms and beyond conventional therapy: the intrinsic multi-enzyme activity of Cu SAzymes is ideal for constructing cascade catalytic systems. Their integration with other modalities (such as photothermal agents, immunomodulators, sonosensitizers, or ferroptosis inducers) can generate potent synergistic effects, overcoming the resistance of single therapy. Furthermore, the antioxidant (SOD/CAT-like) properties should be explored beyond cancer, in areas such as neurodegenerative diseases, rheumatoid arthritis, or ischemia-reperfusion injury, where regulating oxidative stress is crucial.

In conclusion, Cu SAzymes are promising in nanotechnology-based solutions for global health challenges. While their atomic precision offers unprecedented opportunities to simulate and even surpass natural enzymes, moving them from the laboratory to clinical application requires focused efforts to address fundamental translational challenges, such as safety, reproducibility, and controllability. By adopting a multidisciplinary approach that integrates materials science, pharmacology, and clinical insights, Cu SAzymes is poised to transform from an intriguing laboratory spectacle into a reliable next-generation therapeutic and diagnostic drug.

Author contributions

All of the authors contributed to the manuscript preparation. D. P., M. Q., and S. H. conceived the outline of the manuscript. D. P. and S. H. wrote the original draft of the manuscript. Z. Z., X. D., and H. Q. discussed and helped revise the manuscript.

Conflicts of interest

The authors declare that they have no known competing financial interests or personal relationships that could have appeared to influence the work reported in this paper.

Data availability

No primary research results, software, or code have been included, and no new data were generated or analyzed as part of this review. Data available on request from the authors.

Acknowledgements

References

1 W. Wu, L. Huang, E. Wang and S. Dong, *Chem. Sci.*, 2020, **11**, 9741–9756.

2 V. G. Panferov, X. Zhang, K.-Y. Wong, J. H. Lee and J. Liu, *Angew. Chem., Int. Ed.*, 2025, e202512409.

3 X. Li, Z. Wang, J. He, H. Al-Mashriqi, J. Chen and H. Qiu, *Chem. Sci.*, 2025, **16**, 29–42.

4 L. Gao, J. Zhuang, L. Nie, J. Zhang, Y. Zhang, N. Gu, T. Wang, J. Feng, D. Yang, S. Perrett and X. Yan, *Nat. Nanotechnol.*, 2007, **2**, 577–583.

5 Q. Shi, T. Yu, R. Wu and J. Liu, *ACS Appl. Mater. Interfaces*, 2021, **13**, 60815–60836.

6 S. Cai, W. Zhang and R. Yang, *Nano Res.*, 2023, **16**, 13056–13076.

7 Y. Xu, C. Dong, X. Liu, D. Wei, Z. Chen, H. Zhou, J.-b. Li, Y. Yang and W. Tan, *Small*, 2025, e05750.

8 J. Shen, J. Chen, Y. Qian, X. Wang, D. Wang, H. Pan and Y. Wang, *Adv. Mater.*, 2024, **36**, 2313406.

9 C. Peng, R. Pang, J. Li and E. Wang, *Adv. Mater.*, 2024, **36**, 2211724.

10 L. Huang, J. Chen, L. Gan, J. Wang and S. Dong, *Sci. Adv.*, 2019, **5**, eaav5490.

11 X. Yu, Y. Wang, J. Zhang, J. Liu, A. Wang and L. Ding, *Adv. Healthcare Mater.*, 2024, **13**, 2302023.

12 R. Yan, Y. Li and N. Gu, *ACS Appl. Nano Mater.*, 2025, **8**, 15419–15440.

13 Y. Li, X. Hu and H. Deng, *Colloids Surf., B*, 2025, **256**, 115032.

14 C. Deng, Z. Ye, C. J. Zheng, H. Cheng and J. Ge, *Nanoscale*, 2025, **17**, 14103–14117.

15 J. Zhao, F. Han, C. Cheng, H. Wang, G. Zhao, P. Jia, N. Zhang, Y. Wang, J. Zhang and Q. Wei, *Microchem. J.*, 2024, **207**, 111731.

16 Q. Wu, G. Zheng, L. Li and L. Wang, *Adv. Funct. Mater.*, 2025, 2422588.

17 X. Lu, S. Gao, H. Lin, L. Yu, Y. Han, P. Zhu, W. Bao, H. Yao, Y. Chen and J. Shi, *Adv. Mater.*, 2020, **32**, 2002246.

18 B. Xu, S. Li, A. Han, Y. Zhou, M. Sun, H. Yang, L. Zheng, R. Shi and H. Liu, *Adv. Mater.*, 2024, **36**, 2312024.

19 R. Niu, Y. Liu, B. Xu, R. Deng, S. Zhou, Y. Cao, W. Li, H. Zhang, H. Zheng, S. Song, Y. Wang and H. Zhang, *Adv. Mater.*, 2024, **36**, 2312124.

20 Z. H. Zhang, H. Xue, Y. Xiong, Y. T. Geng, A. C. Panayi, S. Knoedler, G. D. Dai, M. A. Shahbazi, B. B. Mi and G. H. Liu, *Theranostics*, 2024, **14**, 547–570.

21 S. Han, L. Xu, Y. Fang and S. Dong, *Chem. Commun.*, 2024, **60**, 12738–12741.

22 Y. He, Y. Chen, X. Yang, C. Song, X. Shen, S. Ma, J. Sun, F. Gao and L. Wang, *Chem. Commun.*, 2025, **61**, 7871–7874.

23 R. Zhang, X. Yan, L. Gao and K. Fan, *Nat. Commun.*, 2025, **16**, 6817.

24 Y. Wang, Y. Wang, L. Y. S. Lee and K.-Y. Wong, *Nanoscale*, 2023, **15**, 18173–18183.

25 J. Li, X. Cai, P. Jiang, H. Wang, S. Zhang, T. Sun, C. Chen and K. Fan, *Adv. Mater.*, 2024, **36**, 2307337.

26 S.-S. Li, A.-J. Wang, P.-X. Yuan, L.-P. Mei, L. Zhang and J.-J. Feng, *Chem. Sci.*, 2022, **13**, 5505–5530.

27 D. Peng, M. Que, S. Huang, S. Wei, N. Wang, Q. He, Z. Zhou and H. Qiu, *Trends Anal. Chem.*, 2026, **194**, 118530.

28 H. Goel, I. Rana, K. Jain, K. R. Ranjan and V. Mishra, *J. Mater. Chem. B*, 2024, **12**, 10466–10489.

29 J. Pei, R. Zhao, X. Mu, J. Wang, C. Liu and X.-D. Zhang, *Biomater. Sci.-UK*, 2020, **8**, 6428–6441.

30 F. Meng, P. Zhu, L. Yang, L. Xia and H. Liu, *Chem. Eng. J.*, 2023, **452**, 139411.

31 Z. Lyu, J. Zhou, S. Ding, D. Du, J. Wang, Y. Liu and Y. Lin, *Trends Anal. Chem.*, 2023, **168**, 117280.

32 C.-N. Zhu, X. Chen, Y.-Q. Xu, F. Wang, D.-Y. Zheng, C. Liu, X.-H. Zhang, Y. Yi and D.-B. Cheng, *ACS Biomater. Sci. Eng.*, 2024, **10**, 7352–7371.

33 S. Zhang, W. Ruan and J. Guan, *Food Chem.*, 2024, **456**, 140094.

34 Q. Wei, Y. Pan, Z. Zhang, S. Yan and Z. Li, *Chem. Eng. J.*, 2024, **483**, 149040.

35 Q. Han, X. Chen, K. Li, H. Huang and Y. Li, *Trends Environ. Anal. Chem.*, 2025, **48**, e00281.

36 X. Dai, H. Liu, B. Cai, Y. Liu, K. Song, J. Chen, S.-Q. Ni, L. Kong and J. Zhan, *Small*, 2023, **19**, 2303901.

37 X. Fan, Y. Gao, F. Yang, J. L. Low, L. Wang, B. Paulus, Y. Wang, A. Trampuz, C. Cheng and R. Haag, *Adv. Funct. Mater.*, 2023, **33**, 2301986.

38 X. Wang, Q. Chen, Y. Zhu, K. Wang, Y. Chang, X. Wu, W. Bao, T. Cao, H. Chen, Y. Zhang and H. Qin, *Signal Transduction Targeted Ther.*, 2023, **8**, 277.

39 P. G. Le, X. A. Le, H. S. Duong, S. H. Jung, T. Kim and M. I. Kim, *Biosens. Bioelectron.*, 2024, **255**, 116259.

40 Y. Zhong, X. Li, P. Qi, C. Sun and Z. Wang, *Nanotechnology*, 2024, **35**, 135102.

41 J. Zhu, Q. Li, X. Li, X. Wu, T. Yuan and Y. Yang, *Langmuir*, 2022, **38**, 6860–6870.

42 J. Bai, Y. Feng, W. Li, Z. Cheng, J. M. Rosenholm, H. Yang, G. Pan, H. Zhang and D. Geng, *Research*, 2023, **6**, 0031.

43 X. Niu, L. Wu, F. Wu, J. Guan and H. Wang, *Biosens. Bioelectron.*, 2023, **238**, 115606.

44 J. Wang, R. Huang, W. Qi, R. Su, B. P. Binks and Z. He, *Appl. Catal., B*, 2019, **254**, 452–462.

45 E. M. Hamed, L. He, V. Rai, S. Hu and S. F. Y. Li, *Small*, 2024, **20**, 2405986.

46 L. Huang, H. Pu and D.-W. Sun, *Small*, 2024, **20**, 2407747.

47 Y. Wu, Y. Tang, W. Xu, R. Su, Y. Qin, L. Jiao, H. Wang, X. Cui, L. Zheng, C. Wang, L. Hu, W. Gu, D. Du, Y. Lin and C. Zhu, *Small*, 2023, **19**, 2302929.

48 L. Wu, H. Lin, X. Cao, Q. Tong, F. Yang, Y. Miao, D. Ye and Q. Fan, *Angew. Chem., Int. Ed.*, 2024, **63**, e202405937.

49 B. Xu, R. Niu, R. Deng, Y. Tang, C. Wang and Y. Wang, *Adv. Funct. Mater.*, 2024, **34**, 2405265.

50 S. Dai, L. Jiang, L. Liu, Z. Su, L. Yao, P. Yang and N. Huang, *Regen. Biomater.*, 2024, **11**, rbae119.

51 X. Qiu, L. Zhuang, J. Yuan, H. Wang, X. Dong, S. He, S. Guan, Z. Chang, P. Bao and J. Colloid Interf, *Sci*, 2023, **652**, 1712–1725.

52 J. Yang, R. Zhang, H. Zhao, H. Qi, J. Li, J.-F. Li, X. Zhou, A. Wang, K. Fan, X. Yan and T. Zhang, *Exploration*, 2022, **2**, 20210267.

53 M. Lu, J. Wang, G. Ren, F. Qin, Z. Zhao, K. Li, W. Chen and Y. Lin, *Nano Res.*, 2022, **15**, 8804–8809.

54 H. Zhou, H. Peng, Y. Lian, T. Sun, C. Su and Z. Wang, *Nano Res.*, 2025, **18**, 94907292.

55 J. Wu, X. Zhu, Q. Li, Q. Fu, B. Wang, B. Li, S. Wang, Q. Chang, H. Xiang, C. Ye, Q. Li, L. Huang, Y. Liang, D. Wang, Y. Zhao and Y. Li, *Nat. Commun.*, 2024, **15**, 6174.

56 Y. Chen, H. Zou, B. Yan, X. Wu, W. Cao, Y. Qian, L. Zheng and G. Yang, *Adv. Sci.*, 2022, **9**, 2103977.

57 Y. Liu, H. Zhao, R. Niu, B. Zhang, B. T. G. Lim, S. Song, Y. Wang, H. Zhang and Y. Zhao, *Chem*, 2025, **11**, 102297.

58 W. Zhang, M. Wang, B. Liu, H. Chen, J. Tan, Q. Meng, J. Li, B. Ding, P. a. Ma and J. Lin, *Angew. Chem., Int. Ed.*, 2024, **63**, e202402397.

59 Y. Pan, Y. Zhang, D. Sun, L. Kong, Y. Liu, D. Yu, K. Song, S. Ni, W. Jiang and J. Zhan, *Adv. Funct. Mater.*, 2025, 2509879.

60 Y. Gao, B. Pan, Y. Wang and Z. Zhu, *Chem. Commun.*, 2025, **61**, 7466–7469.

61 M. Yuan, K. Han, H. Yang, L. Mi, C. Huang, X. Hu and F. He, *Small*, 2024, **20**, 2401756.

62 Y. Pan, Y. Zhang, D. Sun, L. Kong, Y. Liu, D. Yu, K. Song, S. Ni, W. Jiang and J. Zhan, *Adv. Funct. Mater.*, 2025, 2509879.

63 J. Zhong, X. Yang, S. Gao, J. Luo, J. Xiang, G. Li, Y. Liang, L. Tang, C. Qian, J. Zhou, L. Zheng, K. Zhang and J. Zhao, *Adv. Funct. Mater.*, 2023, **33**, 2209399.

64 L. Hu, L. Jiao, C. Chen, X. Jia, X. Li, D. Yan, Y. Zhai and X. Lu, *Anal. Chem.*, 2025, **97**, 1767–1774.

65 Z. Yan, X. Wu, W. Tan, J. Yan, J. Zhou, S. Chen, J. Miao, J. Cheng, C. Shuai and Y. Deng, *Adv. Healthcare Mater.*, 2024, **13**, 2304595.

66 J. Zhou, D. Xu, G. Tian, Q. He, X. Zhang, J. Liao, L. Mei, L. Chen, L. Gao, L. Zhao, G. Yang, W. Yin, G. Nie and Y. Zhao, *J. Am. Chem. Soc.*, 2023, **145**, 4279–4293.

67 H. Ou, Y. Qian, L. Yuan, H. Li, L. Zhang, S. Chen, M. Zhou, G. Yang, D. Wang and Y. Wang, *Adv. Mater.*, 2023, **35**, 2305077.

68 W. Tang, Y. Fang, L. Xie, W. Cai, G. Liu, Y. Lu, Y. Guan, W. Xue, J. Zhao and S. Yu, *Adv. Healthcare Mater.*, 2025, 2405009.

69 X. Xie, X. Chen, Y. Wang, M. Zhang, Y. Fan and X. Yang, *Talanta*, 2023, **257**, 124387.

70 H. Liu, B. Yu, J. Shi, X. Peng, W. Zhou, K. Wang, X. Zhang and H. Wang, *Chem. Eng. J.*, 2024, **480**, 148273.

71 X. Wang, Q. Shi, Z. Zha, D. Zhu, L. Zheng, L. Shi, X. Wei, L. Lian, K. Wu and L. Cheng, *Bioact. Mater.*, 2021, **6**, 4389–4401.

72 S. Zhong, C. Xiong, Y. Zhao, S. Yao, Q. Hu, S. Wang, Q. Zhao and L. Li, *Adv. Funct. Mater.*, 2023, **33**, 2305625.

73 J. Chen, Y. Liu, Z. Long, Y. Li and H. Qiu, *Chin. Chem. Lett.*, 2024, **35**, 109463.

74 K. An, X. Li, J. Chen, S. Zhang, J. Xiao, Q. Wang and H. Qiu, *Anal. Methods-UK*, 2024, **16**, 3551–3561.

75 J. Ge, Y. Yuan, H. Yang, R. Deng, Z. Li and Y. Yang, *Mater. Today Chem.*, 2024, **37**, 102037.

76 Y. Jiang, Z. Chen, Y. Yuan, L. Tian, C. Dong, W. Shen, J. Wei, S. Wang, Y. Yang and J. Ge, *Mater. Today Chem.*, 2024, **41**, 102327.

77 X. Liu, F. Wu, X. Zheng, H. Liu, F. Ren, J. Sun, H. Ding, R. Yang and L. Jin, *ACS Appl. Nano Mater.*, 2023, **6**, 10303–10311.

78 X. Yang, X. Xie, L. Jiang, Y. Fan, C. Zhang and Y. Wang, *Talanta*, 2025, **283**, 127131.

79 Y. Wei, Q. Bai, X. Ning, X. Bai, J. Lv and M. Li, *Anal. Bioanal. Chem.*, 2025, **417**, 1081–1092.

80 L. Nie, H. Zhang, W. Kong, R.-M. Kong, E.-S. Zhang, J. Li, Y. Zhao and F. Qu, *Anal. Chem.*, 2024, **96**, 13158–13165.

81 Y. Wu, J. Wu, L. Jiao, W. Xu, H. Wang, X. Wei, W. Gu, G. Ren, N. Zhang, Q. Zhang, L. Huang, L. Gu and C. Zhu, *Anal. Chem.*, 2020, **92**, 3373–3379.

82 M. Zhang, G. Wang, J. Chen and X. Lu, *Anal. Chim. Acta*, 2024, **1307**, 342628.

83 M.-X. Liu, W.-Y. Liu, H.-Y. Wang and Y.-L. Yu, *Chem. Commun.*, 2025, **61**, 4812–4815.

84 R. Liu, C. Li, L. Zhu, S. Wang, D. Liu, L. Xie, S. Ge and J. Yu, *Anal. Chem.*, 2024, **96**, 12838–12845.

85 H. Liao, J. Li, F. Wang, Y. Chen, W. Deng, B. Li, J. Liu, D. Qian and G. I. N. Waterhouse, *Biosens. Bioelectron.*, 2025, **280**, 117454.

86 Z. Wan, Q. Liu, Y. Zhe, J. Li, D. Ding, S. Liu, H. Wang, H. Qiao, J. Yang, S. Zhang and X. Mu, *Biomater. Sci.-UK*, 2025, **13**, 1033–1044.

87 M. Yu, P. Li, J. Li, X. Chen, Z. Hu, Y. Wang, J. Zeng, F. Han, X. Gong, B. Li and X. Xing, *Adv. Healthcare Mater.*, 2025, **14**, 2403201.

88 F. Wu, Y. Wang, Y. Li, L. Shi, L. Yuan, Y. Ren, H. C. van der Mei and Y. Liu, *ACS Nano*, 2025, **19**, 10816–10828.

89 Y. Wu, Y. Li, G. Lv and W. Bu, *Chem. Sci.*, 2022, **13**, 2202–2217.

90 X. Cai, Q. Zheng, Y. Wu, X. Cheng and C. Zhu, *Chin. Chem. Lett.*, 2025, 111670.

91 L. Mao, J. Lu, X. Wen, Z. Song, C. Sun, Y. Zhao, F. Huang, S. Chen, D. Jiang, W. Che, C. Zhong, C. Yu, K. Li, X. Lu and J. Shi, *Chem. Soc. Rev.*, 2025, **54**, 6282–6334.

92 Y. Xing, J. Xiu, M. Zhou, T. Xu, M. Zhang, H. Li, X. Li, X. Du, T. Ma and X. Zhang, *ACS Nano*, 2023, **17**, 6789–6799.

93 J. Ye, H. Wang, J. Zheng, S. Ning, D. Zhu, J. Shi and R. Shi, *ACS Appl. Mater. Interfaces*, 2025, **17**, 11752–11763.

94 C. Chen, C. Nandi, Q. Yan, L. Meng, W. Chaoyan, X. Conghua and H. Yu, *Int. J. Nanomed.*, 2024, **19**, 403–414.

95 D. Zhu, R. Ling, H. Chen, M. Lyu, H. Qian, K. Wu, G. Li and X. Wang, *Nano Res.*, 2022, **15**, 7320–7328.

96 X. Luo, Y. Zhou, K. Rao, J. Xiang, S. Ning, D. Zhu, G. Li and H. Chen, *Small*, 2025, **21**, 2411576.

97 T. Chen, X. Luo, L. Zhu, J. Xiang, C. Fang, D. Zhu, G. Li and Y. Duo, *Chem. Eng. J.*, 2023, **467**, 143386.

98 C. Guo, Y. Zhou, X. Zhang, J. Shi, Y. Zu, L. Qi, J. Zhao, Q. Fan, Y. Chen and H. Zhou, *Chem. Commun.*, 2025, **61**, 18096–18099.